

MFAI: A Scalable Bayesian Matrix Factorization Approach to Leveraging Auxiliary Information

Zhiwei Wang¹, Fa Zhang¹, Cong Zheng¹, Xianghong Hu¹, Mingxuan Cai^{*2},
and Can Yang^{*1}

¹Department of Mathematics, The Hong Kong University of Science and
Technology

²Department of Biostatistics, City University of Hong Kong

March 7, 2023

Abstract

In various practical situations, matrix factorization methods suffer from poor data quality, such as high data sparsity and low signal-to-noise ratio (SNR). Here we consider a matrix factorization problem by utilizing auxiliary information, which is massively available in real applications, to overcome the challenges caused by poor data quality. Unlike existing methods that mainly rely on simple linear models to combine auxiliary information with the main data matrix, we propose to integrate gradient boosted trees in the probabilistic matrix factorization framework to effectively leverage auxiliary information (MFAI). Thus, MFAI naturally inherits several salient features of gradient boosted trees, such as the capability of flexibly modeling nonlinear relationships, and robustness to irrelevant features and missing values in auxiliary information. The parameters in MFAI can be automatically determined under the empirical Bayes framework, making it adaptive to the utilization of auxiliary information and immune to overfitting. Moreover, MFAI is computationally efficient and scalable to large-scale datasets by exploiting variational inference. We demonstrate the advantages of MFAI through comprehensive numerical results from simulation studies and real data analysis. Our approach is implemented in the R package *mfair* available at <https://github.com/YangLabHKUST/mfair>.

Keywords: low-rank, matrix completion, empirical Bayes, gradient boosting, movie rating, human brain gene expression

*Corresponding authors

1 Introduction

Matrix factorization (Srebro et al., 2004; Rennie and Srebro, 2005; Salakhutdinov and Mnih, 2007, 2008; Babacan et al., 2012; Wang and Stephens, 2021) is widely used to reveal structures hidden in large-scale data. It has become an important problem in the fields of statistics, machine learning, and applied mathematics because of its broad applications. For example, as motivated by the Netflix problem (Bell and Koren, 2007; Koren et al., 2009), matrix factorization is an effective method for inferring the unobserved entries in a large matrix, which is known as the matrix completion problem (Candès and Recht, 2009; Takács et al., 2009; Cai et al., 2010; Candès and Tao, 2010; Mazumder et al., 2010; Wen et al., 2012; Jain et al., 2013). Matrix factorization can also uncover the underlying structure of datasets from diverse research topics, such as background modeling via low-rank approximation in moving object detection (Zhou et al., 2012, 2014), dimension reduction and adjustment for confounding variations (Yang et al., 2013; Lin et al., 2016).

Although existing matrix factorization methods have been used in various applications, major challenges still remain owing to low-quality data arising in practice. First, the observed matrix can be very sparse for the matrix completion problem (Agarwal and Chen, 2009). For example, the MovieLens 100K dataset (Harper and Konstan, 2015) has only 100K observed ratings of 1,682 movies from 943 users, resulting in 94% of entries missing in the rating matrix. Such a high sparsity issue in matrix completion limits the accuracy of matrix factorization methods. Second, the observed matrix can be quite noisy, and matrix factorization in the low signal-to-noise (SNR) settings tends to easily overfit (Mazumder et al., 2010). Effective extraction of signals in the low SNR setting becomes critical for the success of matrix factorization.

A promising way to overcome the above challenges is to leverage auxiliary information (Singh and Gordon, 2008; Xu et al., 2013; Agarwal and Chen, 2009; Porteous et al., 2010; Park et al., 2013; Fithian and Mazumder, 2018), which is massively available in real applications (Agarwal and Chen, 2009; Zakeri et al., 2018; Velten et al., 2022; Shang and Zhou, 2022). For example, besides the main matrix of movie ratings, information about users and movies is often available, including user profiles and descriptive words for movies. To date,

there have been a number of studies on matrix factorization with auxiliary information (Fithian and Mazumder, 2018). These methods can be roughly grouped into two categories: regularized methods and Bayesian methods. For regularized methods, they often assume some shared structures between auxiliary information and the main matrix such that auxiliary information can be incorporated to regularize the factorization of the main matrix. This strategy can be very helpful when the observed data matrix is sparse or in a low SNR regime. To name a few, collective matrix factorization (CMF) (Singh and Gordon, 2008) jointly factorizes the main matrix along with the auxiliary information matrix, assuming they share some latent factors. Inductive matrix completion (IMC) (Xu et al., 2013) assumes that the main matrix lies in the subspace spanned by the auxiliary information matrix. For Bayesian methods, they often build a probabilistic model where auxiliary information is incorporated through a linear model. For example, regression-based latent factor models (RLFM) (Agarwal and Chen, 2009) assume that the latent factor matrices are generated from the auxiliary information via linear regression. Bayesian matrix factorization with side information (BMFSI) (Porteous et al., 2010) augments the factor matrices with additional terms that incorporate auxiliary information using a linear model.

Despite many efforts in the incorporation of auxiliary information, several main issues still remain. First, existing methods rely on linear models to combine auxiliary information with the main matrix, which may limit its role because linear models are not flexible enough. A more flexible framework is highly desired to fully make use of auxiliary information. Second, the computational costs of existing methods are often quite expensive, even though only linear models are used. For example, Bayesian methods often use sampling methods to approximate posterior distributions, such as Markov Chain Monte Carlo (MCMC) (Neal, 1993). However, sampling methods are often too computationally expensive to scale up to large-scale problems. For regularized methods, as pointed out by Hubbard and Hegde (2017) and Zilber and Nadler (2022), parallelization is more challenging for IMC than for standard matrix completion, and an efficient implementation of IMC is still lacking so far. The computational issue will become more serious when we allow more flexible nonlinear models. Third, the incorporation of irrelevant information will not improve but

degrade the performance. Existing methods largely rely on parameter tuning to control the amount of auxiliary information to be incorporated. Although cross-validation helps to tune these parameters, it can be very time-consuming when the number of tuning parameters increases. Statistical methods that can adaptively leverage auxiliary information are highly demanding.

In this article, we develop a scalable Bayesian Matrix Factorization approach to adaptively leveraging Auxiliary Information (MFAI). MFAI allows a flexible nonlinear model to incorporate auxiliary information, enriching its role in the matrix factorization framework. Specifically, MFAI is a unified probabilistic approach to integrating gradient boosted trees (Freund et al., 1996; Breiman, 1998; Friedman et al., 2000; Mason et al., 1999; Friedman, 2001; Bühlmann and Hothorn, 2007; Sigrist, 2021) with matrix factorization. Through innovations in the model and algorithm designs, MFAI has several unique advantages over existing matrix factorization methods. First, MFAI naturally inherits several salient features of gradient boosted trees, such as the capability of flexibly modeling nonlinear relationships, robustness to irrelevant features and missing values in predictors, and ranking the relative importance of auxiliary information which offers more interpretable insights (Elith et al., 2008; Sigrist, 2022a,b; Grinsztajn et al., 2022). Second, the parameters in MFAI can be automatically determined under the empirical Bayes framework, making it adaptive to the utilization of auxiliary information. Third, MFAI is computationally efficient and scalable to large datasets by exploiting variational inference (VI) (Bishop, 2006; Blei et al., 2017). Through comprehensive simulation experiments and real data studies, we demonstrate that MFAI can perform better in matrix factorization and completion tasks than the existing methods. The R package *mfair* is available at <https://github.com/YangLabHKUST/mfair>, serving as a user-friendly tool for matrix factorization with auxiliary information.

2 Methods

2.1 The MFAI Model

Given the main data matrix $\mathbf{Y} \in \mathbb{R}^{N \times M}$ of N samples and M features, we consider the following matrix factorization problem

$$\mathbf{Y} = \mathbf{Z}\mathbf{W}^T + \boldsymbol{\epsilon}, \quad (1)$$

where $\mathbf{Z} \in \mathbb{R}^{N \times K}$ and $\mathbf{W} \in \mathbb{R}^{M \times K}$ are two matrices, and $\boldsymbol{\epsilon} \in \mathbb{R}^{N \times M}$ is a matrix of residual error terms. Here we adopt the terminology of factor analysis and refer to \mathbf{Z} as the “loadings”, \mathbf{W} as the “factors”, and K as the number of factors. We can further expand the above formulation as the sum of the K factors

$$\mathbf{Y} = \sum_{k=1}^K \mathbf{Z}_{\cdot k} \mathbf{W}_{\cdot k}^T + \boldsymbol{\epsilon}, \quad (2)$$

where $\mathbf{Z}_{\cdot k}$ and $\mathbf{W}_{\cdot k}$ are the k -th column of \mathbf{Z} and \mathbf{W} , respectively. Let’s take a user-movie rating matrix \mathbf{Y} as an example, where the observed entry \mathbf{Y}_{nm} represents the rating score of user n for movie m . We may assume that the K factors represent the K traits of movies, where $\mathbf{W}_{\cdot k}$ corresponds to the scores of M movies related to the k -th trait (e.g., action or emotional), $\mathbf{Z}_{\cdot k}$ corresponds to the preference of N users on the k -th trait. The product of preference and score on the k -th trait measures the strength of the k -th factor. The final rating depends on the overall effects of K factors. To perform matrix factorization of \mathbf{Y} , we not only have observed entries in the main matrix but also some auxiliary information. For example, we often have user information $\mathbf{X} \in \mathbb{R}^{N \times C}$ in the above movie rating case, where each row also represents a user with C covariates, such as gender, age, and occupation. We incorporate auxiliary information into matrix factorization by assuming that the users’ preferences are associated with their covariates. Specifically, we relate $\mathbf{Z}_{\cdot k}$ and covariates \mathbf{X} using the following probabilistic model

$$\mathbf{Z}_{\cdot k} \sim \mathcal{N}_N (F_k(\mathbf{X}), \beta_k^{-1} \mathbf{I}_N), \quad k = 1, \dots, K, \quad (3)$$

where $F_k(\mathbf{X}) \in \mathbb{R}^{N \times 1}$ is the mean vector of the loading $\mathbf{Z}_{\cdot k}$, β_k is the precision, $\mathbf{I}_N \in \mathbb{R}^{N \times N}$ is an identity matrix, and $\mathcal{N}_N(\boldsymbol{\mu}, \boldsymbol{\Sigma})$ denotes the N -variate Gaussian distribution with mean

$\boldsymbol{\mu}$ and variance $\boldsymbol{\Sigma}$. Note that $F_k(\mathbf{X})$ is the row-wise evaluation of the unknown function $F_k : \mathbb{R}^C \rightarrow \mathbb{R}$, $F_k(\mathbf{X}) = (F_k(\mathbf{X}_1), \dots, F_k(\mathbf{X}_N))^T$, where $\mathbf{X}_n = (\mathbf{X}_{n1}, \dots, \mathbf{X}_{nC})^T \in \mathbb{R}^{C \times 1}$ is the n -th row of \mathbf{X} containing auxiliary information for the n -th sample, $n = 1, \dots, N$. Regarding $F_k(\cdot)$, it is often assumed to be a linear function, $F_k(\mathbf{X}_n) = \gamma_0 + \mathbf{X}_n^T \boldsymbol{\gamma}$, where γ_0 is the intercept and $\boldsymbol{\gamma} \in \mathbb{R}^{C \times 1}$ represents regression coefficients. However, the linearity assumption can be too simplified to characterize a flexible relationship between $\mathbf{Z}_{\cdot k}$ and \mathbf{X} . In the MFAI model, we assume that $F_k(\cdot)$ in (3) is a nonlinear function represented by a tree ensemble,

$$F_k(\cdot) = \sum_{t=1}^{T_k} f_k^t(\cdot), \quad (4)$$

where $f_k^t(\cdot)$ is a regression tree (Breiman et al., 1984), and T_k is the total number of trees. The advantages of the proposed model are threefold. First, tree ensembles are able to capture a more flexible relationship between loading $\mathbf{Z}_{\cdot k}$ and auxiliary information \mathbf{X} . Second, the proposed model naturally inherits several salient features of regression trees, such as ranking variable importance and handling missing values. Third, we can develop an efficient algorithm to estimate the nonlinear model from data and make it scalable to large-scale matrix factorization. We then assign an independent Gaussian prior for the corresponding k -th factor $\mathbf{W}_{\cdot k}$

$$\mathbf{W}_{\cdot k} \sim \mathcal{N}_M(0, \mathbf{I}_M), \quad (5)$$

and for independent error terms $\boldsymbol{\epsilon}$ as

$$\epsilon_{nm} \sim \mathcal{N}(0, \tau^{-1}), \quad n = 1, \dots, N \text{ and } m = 1, \dots, M, \quad (6)$$

where τ is the precision of ϵ_{nm} . In the MFAI model, \mathbf{Z} and \mathbf{W} are often referred to as latent variables in the statistical machine learning literature.

Let $\boldsymbol{\theta} = \{\tau, \boldsymbol{\beta}\} = \{\tau; \beta_1, \dots, \beta_K\}$ be the collection of model parameters and $\mathbf{F}(\cdot) = \{F_1(\cdot), \dots, F_K(\cdot)\}$ be the collection of K unknown functions. Combining model (2) (3) (5) (6), we can write down the joint probabilistic model as

$$\begin{aligned} \Pr(\mathbf{Y}, \mathbf{Z}, \mathbf{W} \mid \boldsymbol{\theta}, \mathbf{F}(\cdot)) &= \Pr(\mathbf{Y} \mid \mathbf{Z}, \mathbf{W}; \tau) \Pr(\mathbf{Z} \mid \boldsymbol{\beta}, \mathbf{F}(\cdot)) \Pr(\mathbf{W}) \\ &= \Pr(\mathbf{Y} \mid \mathbf{Z}, \mathbf{W}; \tau) \prod_{k=1}^K \Pr(\mathbf{Z}_{\cdot k} \mid \beta_k, F_k(\cdot)) \prod_{k=1}^K \Pr(\mathbf{W}_{\cdot k}). \end{aligned} \quad (7)$$

As an empirical Bayes approach, we can adaptively estimate parameters $\boldsymbol{\theta}$ and the unknown functions $\mathbf{F}(\cdot)$ by optimizing the log marginal likelihood

$$\begin{aligned} (\hat{\boldsymbol{\theta}}, \hat{\mathbf{F}}(\cdot)) &= \arg \max_{\boldsymbol{\theta}, \mathbf{F}(\cdot)} \log \Pr(\mathbf{Y} \mid \boldsymbol{\theta}, \mathbf{F}(\cdot)) \\ &= \arg \max_{\boldsymbol{\theta}, \mathbf{F}(\cdot)} \log \int \Pr(\mathbf{Y}, \mathbf{Z}, \mathbf{W} \mid \boldsymbol{\theta}, \mathbf{F}(\cdot)) d\mathbf{Z} d\mathbf{W}. \end{aligned} \quad (8)$$

Then we can infer the latent loadings and factors by obtaining their posterior probability as

$$\Pr(\mathbf{Z}, \mathbf{W} \mid \mathbf{Y}; \hat{\boldsymbol{\theta}}, \hat{\mathbf{F}}(\cdot)) = \frac{\Pr(\mathbf{Y}, \mathbf{Z}, \mathbf{W} \mid \hat{\boldsymbol{\theta}}, \hat{\mathbf{F}}(\cdot))}{\Pr(\mathbf{Y} \mid \hat{\boldsymbol{\theta}}, \hat{\mathbf{F}}(\cdot))}. \quad (9)$$

2.2 Fitting the MFAI Model

We begin our algorithm design with the single-factor case, i.e., $K = 1$, and extend our algorithm to the multi-factor case in Section 2.2.4. The single-factor MFAI model is as follows

$$\begin{aligned} \mathbf{Y} &= \mathbf{z}\mathbf{w}^T + \boldsymbol{\epsilon}, \\ \mathbf{z} &\sim \mathcal{N}_N(F(\mathbf{X}), \beta^{-1}\mathbf{I}_N), \\ \mathbf{w} &\sim \mathcal{N}_M(0, \mathbf{I}_M), \\ \epsilon_{nm} &\sim \mathcal{N}(0, \tau^{-1}), \quad n = 1, \dots, N \text{ and } m = 1, \dots, M, \end{aligned} \quad (10)$$

where $\mathbf{z} \in \mathbb{R}^{N \times 1}$, $\mathbf{w} \in \mathbb{R}^{M \times 1}$, and $F(\mathbf{X}) \in \mathbb{R}^{N \times 1}$ denotes $(F(\mathbf{X}_1), \dots, F(\mathbf{X}_N))^T$. Then the joint probabilistic model becomes

$$\Pr(\mathbf{Y}, \mathbf{z}, \mathbf{w} \mid \boldsymbol{\theta}, F(\cdot)) = \Pr(\mathbf{Y} \mid \mathbf{z}, \mathbf{w}; \tau) \Pr(\mathbf{z} \mid \beta, F(\cdot)) \Pr(\mathbf{w}), \quad (11)$$

where $\boldsymbol{\theta} = \{\tau, \beta\}$ is the collection of model parameters and $F(\cdot)$ is an unknown function. The goal is to estimate $\boldsymbol{\theta}$ and $F(\cdot)$ by optimizing the log marginal likelihood

$$\begin{aligned} (\hat{\boldsymbol{\theta}}, \hat{F}(\cdot)) &= \arg \max_{\boldsymbol{\theta}, F(\cdot)} \log \Pr(\mathbf{Y} \mid \boldsymbol{\theta}, F(\cdot)) \\ &= \arg \max_{\boldsymbol{\theta}, F(\cdot)} \log \int \Pr(\mathbf{Y}, \mathbf{z}, \mathbf{w} \mid \boldsymbol{\theta}, F(\cdot)) d\mathbf{z} d\mathbf{w}. \end{aligned} \quad (12)$$

The posterior probability of \mathbf{z} and \mathbf{w} is given as

$$\Pr(\mathbf{z}, \mathbf{w} \mid \mathbf{Y}; \hat{\boldsymbol{\theta}}, \hat{F}(\cdot)) = \frac{\Pr(\mathbf{Y}, \mathbf{z}, \mathbf{w} \mid \hat{\boldsymbol{\theta}}, \hat{F}(\cdot))}{\Pr(\mathbf{Y} \mid \hat{\boldsymbol{\theta}}, \hat{F}(\cdot))}. \quad (13)$$

2.2.1 Approximate Bayesian Inference

The Bayesian inference using (12) and (13) is intractable since the marginal likelihood $\Pr(\mathbf{Y} \mid \boldsymbol{\theta}, F(\cdot))$ cannot be computed by marginalizing all latent variables. To tackle the Bayesian inference problem, there are two main methods: Markov Chain Monte Carlo (MCMC) (Neal, 1993), which is a sampling-based approach, and variational inference (VI), which is an approximation-based approach (Bishop, 2006; Blei et al., 2017). The advantage of the sampling-based methods is that they produce exact results asymptotically. In practice, however, they are often too computationally expensive for large-scale problems. Here, we propose a variational expectation-maximization (EM) algorithm to perform approximate Bayesian inference (with details in Appendices Section A.1). To apply variational approximation, we first define $q(\mathbf{z}, \mathbf{w})$ as an approximated distribution of posterior $\Pr(\mathbf{z}, \mathbf{w} \mid \mathbf{Y}; \boldsymbol{\theta}, F(\cdot))$. Then we obtain the evidence lower bound (ELBO) of the logarithm of the marginal likelihood by Jensen’s inequality

$$\begin{aligned} \log \Pr(\mathbf{Y} \mid \boldsymbol{\theta}, F(\cdot)) &= \log \int \Pr(\mathbf{Y}, \mathbf{z}, \mathbf{w} \mid \boldsymbol{\theta}, F(\cdot)) \, d\mathbf{z} \, d\mathbf{w} \\ &\geq \int q(\mathbf{z}, \mathbf{w}) \log \frac{\Pr(\mathbf{Y}, \mathbf{z}, \mathbf{w} \mid \boldsymbol{\theta}, F(\cdot))}{q(\mathbf{z}, \mathbf{w})} \, d\mathbf{z} \, d\mathbf{w} \\ &= \mathbb{E}_q[\log \Pr(\mathbf{Y}, \mathbf{z}, \mathbf{w} \mid \boldsymbol{\theta}, F(\cdot))] - \mathbb{E}_q[\log q(\mathbf{z}, \mathbf{w})] \\ &\equiv \text{ELBO}(q; \boldsymbol{\theta}, F(\cdot)), \end{aligned} \tag{14}$$

where the equality holds if and only if $q(\mathbf{z}, \mathbf{w})$ is the exact posterior $\Pr(\mathbf{z}, \mathbf{w} \mid \mathbf{Y}; \boldsymbol{\theta}, F(\cdot))$. Instead of maximizing the logarithm of the marginal likelihood, we can iteratively maximize the ELBO with respect to the variational approximate posterior q , the model parameters $\boldsymbol{\theta}$, and the function $F(\cdot)$

$$\left(\widehat{q}; \widehat{\boldsymbol{\theta}}, \widehat{F}(\cdot)\right) = \arg \max_{q; \boldsymbol{\theta}, F(\cdot)} \text{ELBO}(q; \boldsymbol{\theta}, F(\cdot)). \tag{15}$$

Using the terminology in the EM algorithm, maximization of ELBO with respect to q is known as the E-step, and maximization of ELBO with respect to $\boldsymbol{\theta}$ and $F(\cdot)$ is known as the M-step.

To approximate the posterior distribution, we consider the following factorization of variational distribution $q(\mathbf{z}, \mathbf{w})$ based on the mean-field theory (Bishop, 2006; Blei et al.,

2017)

$$q(\mathbf{z}, \mathbf{w}) = q(\mathbf{z})q(\mathbf{w}). \quad (16)$$

Without further assumptions, we show that (with details in Appendices Section A.1.1) the optimal solution of $q(\mathbf{z})$ and $q(\mathbf{w})$ in the E-step is given as two multivariate Gaussian distributions

$$q(\mathbf{z}) = \mathcal{N}_N(\mathbf{z} \mid \boldsymbol{\mu}, \mathbf{A}), \quad q(\mathbf{w}) = \mathcal{N}_M(\mathbf{w} \mid \boldsymbol{\nu}, \mathbf{B}), \quad (17)$$

where $\boldsymbol{\mu} \in \mathbb{R}^{N \times 1}$ and $\boldsymbol{\nu} \in \mathbb{R}^{M \times 1}$ are posterior mean vectors, $\mathbf{A} \in \mathbb{R}^{N \times N}$ and $\mathbf{B} \in \mathbb{R}^{M \times M}$ are posterior covariance matrices

$$\mathbf{A} = a^2 \mathbf{I}_N, \quad \mathbf{B} = b^2 \mathbf{I}_M. \quad (18)$$

Now suppose that we are at the t -th step of the variational EM algorithm, and we have obtained variational parameters $\{\boldsymbol{\mu}^{(t-1)}, a^{2(t-1)}; \boldsymbol{\nu}^{(t-1)}, b^{2(t-1)}\}$, model parameters $\boldsymbol{\theta}^{(t-1)} = \{\tau^{(t-1)}, \beta^{(t-1)}\}$, and function $F^{(t-1)}(\cdot)$ at the $(t-1)$ -th step. To maximize ELBO in the t -th E-step, we can update variational parameters as

$$\begin{aligned} a^{2(t)} &= \frac{1}{\beta^{(t-1)} + \tau^{(t-1)} \left(\|\boldsymbol{\nu}^{(t-1)}\|_2^2 + Mb^{2(t-1)} \right)}, \\ \boldsymbol{\mu}^{(t)} &= a^{2(t)} \left(\beta^{(t-1)} F^{(t-1)}(\mathbf{X}) + \tau^{(t-1)} \mathbf{Y} \boldsymbol{\nu}^{(t-1)} \right), \\ b^{2(t)} &= \frac{1}{1 + \tau^{(t-1)} \left(\|\boldsymbol{\mu}^{(t)}\|_2^2 + Na^{2(t)} \right)}, \\ \boldsymbol{\nu}^{(t)} &= b^{2(t)} \tau^{(t-1)} \mathbf{Y}^T \boldsymbol{\mu}^{(t)}, \end{aligned} \quad (19)$$

where $\|\cdot\|_2$ for a vector denotes the Euclidean norm. It is obvious that the variational approximate posterior $q^{(t)}(\mathbf{z}, \mathbf{w})$ only depends on the values of parameters $\{\boldsymbol{\mu}^{(t)}, a^{2(t)}; \boldsymbol{\nu}^{(t)}, b^{2(t)}\}$. We also note that each entry of \mathbf{z} has the same posterior variance $a^{2(t)}$, and \mathbf{w} as well. Under the variational approximation framework, $q^{(t)}(\mathbf{z})$ can be viewed as the approximation to the posterior distribution $\Pr(\mathbf{z} \mid \mathbf{Y}; \boldsymbol{\theta}^{(t-1)}, F^{(t-1)}(\cdot))$, and $q^{(t)}(\mathbf{w})$ can be viewed as the approximation to the posterior distribution $\Pr(\mathbf{w} \mid \mathbf{Y}; \boldsymbol{\theta}^{(t-1)}, F^{(t-1)}(\cdot))$. Naturally, we can infer \mathbf{z} and \mathbf{w} using the posterior mean $\boldsymbol{\mu}^{(t)}$ and $\boldsymbol{\nu}^{(t)}$ after the convergence of the algorithm.

With the variational approximation $q^{(t)}$ updated in the t -th E-step, we can update

model parameters $\boldsymbol{\theta} = \{\tau, \beta\}$ and function $F(\cdot)$ in the M-step

$$\left(\boldsymbol{\theta}^{(t)}, F^{(t)}(\cdot)\right) = \arg \max_{\boldsymbol{\theta}, F(\cdot)} \text{ELBO}(q^{(t)}; \boldsymbol{\theta}, F(\cdot)), \quad (20)$$

where

$$\begin{aligned} & \text{ELBO}\left(q^{(t)}\left(\mathbf{z}, \mathbf{w} \mid \boldsymbol{\mu}^{(t)}, a^{2(t)}; \boldsymbol{\nu}^{(t)}, b^{2(t)}\right); \tau, \beta, F(\cdot)\right) \\ &= \mathbb{E}_{q^{(t)}(\mathbf{z}, \mathbf{w})} [\log \Pr(\mathbf{Y}, \mathbf{z}, \mathbf{w} \mid \boldsymbol{\theta}, F(\cdot))] - \mathbb{E}_{q^{(t)}(\mathbf{z}, \mathbf{w})} [\log q^{(t)}(\mathbf{z}, \mathbf{w})] \\ &= -\frac{\tau}{2} \left(\left\| \mathbf{Y}^{(t)} - \boldsymbol{\mu}^{(t)} \boldsymbol{\nu}^{(t)\top} \right\|_{\text{F}}^2 + \left\| \left(\boldsymbol{\mu}^{(t)2} + \text{diag}(\mathbf{A}^{(t)}) \right) \left(\boldsymbol{\nu}^{(t)2} + \text{diag}(\mathbf{B}^{(t)}) \right)^{\text{T}} - \boldsymbol{\mu}^{(t)2} \left(\boldsymbol{\nu}^{(t)2} \right)^{\text{T}} \right\|_{1,1} \right) \\ & \quad + \frac{NM}{2} \log \tau + \frac{N}{2} \log \beta - \frac{\beta}{2} \left(\left\| \boldsymbol{\mu}^{(t)} - F(\mathbf{X}) \right\|_2^2 + Na^{2(t)} \right) + \text{const}. \end{aligned} \quad (21)$$

Here for a matrix, $\|\cdot\|_{\text{F}}$ denotes the Frobenius norm, and $\|\cdot\|_{1,1}$ denotes the entry-wise matrix norm-sum of the absolute value of all the entries. We first consider optimizing model parameters with the estimate of the function $F^{(t-1)}(\cdot)$ fixed. By solving

$$\left. \frac{\partial \text{ELBO}(q; \boldsymbol{\theta}, F(\cdot))}{\partial \boldsymbol{\theta}} \right|_{q=q^{(t)}, F(\cdot)=F^{(t-1)}(\cdot)} = 0 \quad (22)$$

we obtain the updating equations for parameter estimation in the t -th M-step

$$\begin{aligned} \tau^{(t)} &= \frac{NM}{\left\| \mathbf{Y} - \boldsymbol{\mu}^{(t)} \boldsymbol{\nu}^{(t)\top} \right\|_{\text{F}}^2 + \left\| \left(\boldsymbol{\mu}^{(t)2} + \text{diag}(\mathbf{A}^{(t)}) \right) \left(\boldsymbol{\nu}^{(t)2} + \text{diag}(\mathbf{B}^{(t)}) \right)^{\text{T}} - \boldsymbol{\mu}^{(t)2} \left(\boldsymbol{\nu}^{(t)2} \right)^{\text{T}} \right\|_{1,1}}, \\ \beta^{(t)} &= \frac{N}{\left\| \boldsymbol{\mu}^{(t)} - F^{(t-1)}(\mathbf{X}) \right\|_2^2 + Na^{2(t)}}, \end{aligned} \quad (23)$$

where $\boldsymbol{\mu}^2 \in \mathbb{R}^{N \times 1}$ denotes Hadamard product $\boldsymbol{\mu}^2 = \boldsymbol{\mu} \odot \boldsymbol{\mu}$, and $\text{diag}(\mathbf{A}) \in \mathbb{R}^{N \times 1}$ denotes a vector containing all the entries on the main diagonal of \mathbf{A} . To maximize ELBO with respect to $F(\cdot)$, we propose to update $F(\cdot)$ from its current estimate $F^{(t-1)}(\cdot)$ to its new estimate $F^{(t)}(\cdot)$ by constructing the following additive model

$$F^{(t)}(\cdot) = F^{(t-1)}(\cdot) + f^{(t)}(\cdot), \quad (24)$$

where $f^{(t)}(\cdot)$ is chosen to be a single regression tree (Breiman et al., 1984) in MAFI. Clearly, this leads to the following optimization problem

$$f^{(t)}(\mathbf{X}) = \arg \min_{f(\cdot)} \left\| \boldsymbol{\mu}^{(t)} - F^{(t-1)}(\mathbf{X}) - f(\mathbf{X}) \right\|_2^2, \quad (25)$$

where $\boldsymbol{\mu}^{(t)}$ is given in the t -th E-step and $F^{(t-1)}(\cdot)$ is the current estimated function. After obtaining $f^{(t)}(\cdot)$ from (25), we update $F(\cdot)$ as

$$F^{(t)}(\cdot) = F^{(t-1)}(\cdot) + s \cdot f^{(t)}(\cdot), \quad (26)$$

where $0 < s < 1$ is the so-called shrinkage parameter or learning rate. Clearly, information in the auxiliary matrix is gradually incorporated to modulate the prior of \mathbf{z} , and the corresponding posterior mean will be updated as $\boldsymbol{\mu}^{(t+1)} = a^{2(t)} (\beta^{(t)} F^{(t)}(\mathbf{X}) + \tau^{(t)} \mathbf{Y} \boldsymbol{\nu}^{(t)})$ in the $(t+1)$ -th step.

To summarize, the proposed algorithm is a variational EM algorithm and its convergence is naturally guaranteed. In the E-step, we optimize the variational distribution $q(\mathbf{z}, \mathbf{w})$ to maximize the ELBO. In the M-step, we update the model parameters $\boldsymbol{\theta}$ and function $F(\cdot)$ to optimize the ELBO. The novelty of the proposed algorithm comes from the way we update function $F(\cdot)$, where we combine the gradient boosting strategy (26) into the iterations of our variational EM algorithm. In such a way, the nonlinear relationship between auxiliary information \mathbf{X} and loading \mathbf{z} can be built up in a stage-wise fashion, yielding a very stable way to incorporate auxiliary information in matrix factorization. In the meanwhile, the algorithm fully exploits the advantages of tree-based methods when fitting a single tree $f^{(t)}(\cdot)$ in the t -th step, such as ranking variable importance and handling missing values with trees. Last but not least, our algorithm can be efficient in handling large-scale problems because trees are scalable to large-scale data matrix \mathbf{X} . We denote the proposed algorithm to fit the single-factor model as MFALS F and summarize it in Algorithm 1.

2.2.2 Missing Data

One important feature of MFAI is its ability to handle missing data, either in the main matrix \mathbf{Y} or in the auxiliary matrix \mathbf{X} . To handle \mathbf{Y} with missing entries, we consider the following probabilistic model for the observed entries \mathbf{Y}^{obs} (see details in Appendices Section A.2)

$$\begin{aligned} \Pr(\mathbf{Y}^{\text{obs}} | \boldsymbol{\theta}, F(\cdot)) &= \Pr(\mathbf{Y}^{\text{obs}} | \mathbf{z}, \mathbf{w}; \tau) \Pr(\mathbf{z} | \beta, F(\cdot)) \Pr(\mathbf{w}) \\ &= \prod_{(n,m) \in \Omega^{\text{obs}}} \Pr(\mathbf{Y}_{nm} | \mathbf{z}, \mathbf{w}; \tau) \Pr(\mathbf{z} | \beta, F(\cdot)) \Pr(\mathbf{w}), \end{aligned} \quad (27)$$

Algorithm 1: Fitting the Single-Factor MFAI Model

Data: Main data matrix \mathbf{Y} and auxiliary matrix \mathbf{X}

Result: Estimate of the latent variables $\hat{\mathbf{z}} = \boldsymbol{\mu}$ and $\hat{\mathbf{w}} = \boldsymbol{\nu}$

```

1 initialize posterior  $q^{(0)} = q\left(\boldsymbol{\mu}^{(0)}, a^{2(0)}; \boldsymbol{\nu}^{(0)}, b^{2(0)}\right)$ ;
2 initialize model parameters  $\boldsymbol{\theta}^{(0)} = \{\tau^{(0)}, \beta^{(0)}\}$ ;
3 initialize function  $F^{(0)}(\cdot) \equiv 0$ , then prior means  $F^{(0)}(\mathbf{X}) = 0$ ;
4 set the shrinkage parameter  $s$ ;
5  $t \leftarrow 0$ ;
6 repeat
7    $t \leftarrow t + 1$ ;
8    $\boldsymbol{\mu}^{(t)}, a^{2(t)}; \boldsymbol{\nu}^{(t)}, b^{2(t)} \leftarrow \arg \max_{\boldsymbol{\mu}, a^2; \boldsymbol{\nu}, b^2} \text{ELBO}\left(q\left(\boldsymbol{\mu}, a^2; \boldsymbol{\nu}, b^2\right); \tau^{(t-1)}, \beta^{(t-1)}; F^{(t-1)}(\cdot)\right)$ ;
   // update the variational approximation of posterior
9    $\tau^{(t)}, \beta^{(t)} \leftarrow \arg \max_{\tau, \beta} \text{ELBO}\left(q\left(\boldsymbol{\mu}^{(t)}, a^{2(t)}; \boldsymbol{\nu}^{(t)}, b^{2(t)}\right); \tau, \beta; F^{(t-1)}(\cdot)\right)$ ;
   // update the model parameters
10   $f^{(t)}(\cdot) \leftarrow \arg \max_{f(\cdot)} \text{ELBO}\left(q\left(\boldsymbol{\mu}^{(t)}, a^{2(t)}; \boldsymbol{\nu}^{(t)}, b^{2(t)}\right); \tau^{(t)}, \beta^{(t)}; F^{(t-1)}(\cdot) + f(\cdot)\right)$ ;
   // compute the functional gradient
11   $F^{(t)}(\cdot) \leftarrow F^{(t-1)}(\cdot) + s \cdot f^{(t)}(\cdot)$ ; // update the function
12 until convergence criterion satisfied;
13 return  $\boldsymbol{\mu}^{(t)}, a^{2(t)}; \boldsymbol{\nu}^{(t)}, b^{2(t)}; \tau^{(t)}, \beta^{(t)}; F^{(t)}(\cdot)$ .

```

where Ω^{obs} is the collection of the indices of the observed entries of \mathbf{Y} . Within the approximate Bayesian inference framework, the updating equations for the variational approximate posteriors are similar to (19). For n -th entry of \mathbf{z} , the posterior variance $\mathbf{a}_n^{2(t)}$ and posterior mean $\boldsymbol{\mu}_n^{(t)}$ are updated at the t -th step as

$$\begin{aligned}
 \mathbf{a}_n^{2(t)} &= \frac{1}{\beta^{(t-1)} + \tau^{(t-1)} \sum_{m' \in \Omega_n^{\text{obs}}} \left(\left(\boldsymbol{\nu}_{m'}^{(t-1)} \right)^2 + \mathbf{b}_{m'}^{2(t-1)} \right)}, \\
 \boldsymbol{\mu}_n^{(t)} &= \mathbf{a}_n^{2(t)} \left(\beta^{(t-1)} F^{(t-1)}(\mathbf{X}_{n \cdot}) + \tau^{(t-1)} \sum_{m' \in \Omega_n^{\text{obs}}} \mathbf{Y}_{nm'} \boldsymbol{\nu}_{m'}^{(t-1)} \right),
 \end{aligned} \tag{28}$$

where Ω_n^{obs} denotes the collection of the indices of the observed entries in the n -th row of \mathbf{Y} . Here we can clearly see that auxiliary information has been incorporated for matrix imputation. The posterior mean $\boldsymbol{\mu}_n^{(t)}$ is updated as a weighted average between observed information and current prior information in $F^{(t-1)}(\cdot)$. Importantly, the weights $\beta^{(t-1)}$ and $\tau^{(t-1)}$, as well as prior information $F^{(t-1)}(\cdot)$ are all adaptively estimated from data rather than pre-fixed. Similarly for the m -th entry of \mathbf{w} , the posterior variance $\mathbf{b}_m^{2(t)}$ and posterior mean $\boldsymbol{\nu}_m^{(t)}$ are updated as

$$\begin{aligned}\mathbf{b}_m^{2(t)} &= \frac{1}{1 + \tau^{(t-1)} \sum_{n' \in \Omega_m^{\text{obs}}} \left(\left(\boldsymbol{\mu}_{n'}^{(t-1)} \right)^2 + \mathbf{a}_{n'}^{2(t-1)} \right)}, \\ \boldsymbol{\nu}_m^{(t)} &= \mathbf{b}_m^{2(t)} \tau^{(t-1)} \sum_{n' \in \Omega_m^{\text{obs}}} \mathbf{Y}_{n'm} \boldsymbol{\mu}_{n'}^{(t-1)},\end{aligned}\tag{29}$$

where Ω_m^{obs} denotes the collection of the indices of the observed entries in m -th column of \mathbf{Y} . Regarding the model parameters, they can be updated as

$$\begin{aligned}\tau^{(t)} &= \frac{|\Omega^{\text{obs}}|}{\left\| \mathcal{P}_{\Omega^{\text{obs}}} \left(\mathbf{Y} - \boldsymbol{\mu}^{(t)} \boldsymbol{\nu}^{(t)\text{T}} \right) \right\|_{\text{F}}^2 + \left\| \mathcal{P}_{\Omega^{\text{obs}}} \left(\left(\boldsymbol{\mu}^{(t)^2} + \mathbf{a}^{2(t)} \right) \left(\boldsymbol{\nu}^{(t)^2} + \mathbf{b}^{2(t)} \right)^{\text{T}} - \boldsymbol{\mu}^{(t)^2} \left(\boldsymbol{\nu}^{(t)^2} \right)^{\text{T}} \right) \right\|_{1,1}}, \\ \beta^{(t)} &= \frac{N}{\left\| \boldsymbol{\mu}^{(t)} - F^{(t-1)}(\mathbf{X}) \right\|_2^2 + \left\| \mathbf{a}^{2(t)} \right\|_1},\end{aligned}\tag{30}$$

where \mathcal{P} is a projection operator and $\mathcal{P}_{\Omega}(\mathbf{Y})$ outputs a matrix with the same dimension as that of \mathbf{Y}

$$(\mathcal{P}_{\Omega}(\mathbf{Y}))_{nm} = \begin{cases} \mathbf{Y}_{nm}, & \text{if } (n, m) \in \Omega, \\ 0, & \text{otherwise.} \end{cases}\tag{31}$$

The update for the function $F(\cdot)$ remains the same as (25) and (26). As for the missing data in auxiliary information, it is clear that only the update steps involving the auxiliary matrix \mathbf{X} need to be reconsidered. Utilizing the *rpart* package (Therneau and Atkinson, 2022a), any observation with value for the dependent variable (i.e., $\boldsymbol{\mu}_n$) and at least one independent variable (i.e., one of $\{\mathbf{X}_{n1}, \dots, \mathbf{X}_{nC}\}$) will participate in the modeling. For each split, the observation with the missing split variable will be split based on the best surrogate variable; if that's missing, then by the next best, and so on (Therneau and Atkinson, 2022b).

2.2.3 Ranking the Importance of Auxiliary Covariates

Auxiliary covariates may not be equally important for identifying the loading \mathbf{z} . In a single tree, the importance of a variable is given by the total goodness of all the splits, either as a primary or a surrogate variable. Specifically, an overall measure of variable importance is the sum of the goodness for each split in which it was the primary variable, then plus the adjusted goodness for all splits in which it was a surrogate (Therneau and Atkinson, 2022b). The higher the importance value is, the more the variable contributes to improving the model. By inheriting the merit of regression trees, the model given by MFAI can be used to rank the importance of auxiliary covariates. Suppose the variable importance of the c -th covariate (i.e., $\mathbf{X}_{\cdot c}$) in the t -th tree (i.e., $f^t(\cdot)$) is \mathcal{I}_{tc} , then the total importance score is given by

$$\mathcal{I}_c = \sum_{t=1}^T \mathcal{I}_{tc}, \quad (32)$$

where T is the total number of trees contained in the model.

2.2.4 The K -factor MFAI Model

Now we extend the single-factor approach to fit the K -factor MFAI model specified by equations (2) - (6). To do so, we introduce the variational approximations $\{q(\mathbf{Z}_{\cdot k}), q(\mathbf{W}_{\cdot k})\}$ for $k = 1, \dots, K$, and then optimize $\text{ELBO}(q(\mathbf{Z}_{\cdot 1}, \mathbf{W}_{\cdot 1}), \dots, q(\mathbf{Z}_{\cdot K}, \mathbf{W}_{\cdot K}); \tau, \beta_1, \dots, \beta_K, F_1(\cdot), \dots, F_K(\cdot))$. Similar to the single-factor case, the optimization can be done by iteratively updating parameters relating to a single factor while keeping others fixed. The updates of a single pair $\{\mathbf{Z}_{\cdot k}, \mathbf{W}_{\cdot k}\}$ are essentially identical to those for fitting the single-factor model aforementioned, except that \mathbf{Y} is replaced with the residuals obtained by removing the estimated effects of the other $K - 1$ pairs

$$\mathbf{R}^k := \mathbf{Y} - \sum_{k' \neq k} \mathbf{Z}_{\cdot k'} \mathbf{W}_{\cdot k'}^T. \quad (33)$$

We implement two algorithms for fitting the K -factor MFAI model: the greedy algorithm and the backfitting algorithm. The greedy algorithm starts by fitting the single-factor model and then adds factors $k = 2, \dots, K$, one at a time, optimizing over the new factor parameters before moving on to the next factor. The backfitting algorithm (Breiman and

Friedman, 1985) iteratively refines the estimates for each factor given the estimates for the other factors. In our MFAI framework, we choose to use the greedy algorithm first to provide rough estimates (for all of the variational approximations, model parameters, and unknown functions) as the initialization for the backfitting algorithm. The greedy and backfitting algorithms are summarized in Algorithm 2 and 3, respectively.

Algorithm 2: Greedy Algorithm for K -Factor MFAI Model

Data: Main data matrix \mathbf{Y} and auxiliary matrix \mathbf{X}

Result: Estimate of the latent loadings \mathbf{Z} and factors \mathbf{W}

```

1 for  $k = 1, \dots, K$  do
2    $\boldsymbol{\mu}_k, a_k^2; \boldsymbol{\nu}_k, b_k^2; \tau_k, \beta_k; F_k(\cdot) \leftarrow \text{MFAISF}(\mathbf{Y}, \mathbf{X})$ ;
3    $\mathbf{Y} \leftarrow \mathbf{Y} - \boldsymbol{\mu}_k \boldsymbol{\nu}_k^T$ ;
4 end
5 return  $\widehat{\mathbf{Z}} = (\boldsymbol{\mu}_1, \dots, \boldsymbol{\mu}_K), \widehat{\mathbf{W}} = (\boldsymbol{\nu}_1, \dots, \boldsymbol{\nu}_K); a_1^2, \dots, a_K^2, b_1^2, \dots, b_K^2$ ;
6 return  $\tau_1, \dots, \tau_K; \beta_1, \dots, \beta_K$ ;
7 return  $F_1(\cdot), \dots, F_K(\cdot)$ .
```

A practical issue of matrix factorization is how to select the number of factors K . Regularized methods often rely on technology such as cross-validation, which can introduce high computational costs. In contrast, taking the advantage of additive model and the stage-wise manner to fit the K -factor model sequentially (as shown in Algorithm 2), MFAI can automatically determine K with a little modification on the algorithm. We first set the maximum value of the number of factors K_{\max} and perform the for-loop in the greedy algorithm 2 with K replaced by K_{\max} . In this process, if we find the k -th loading/factor combination $\boldsymbol{\mu}_k \boldsymbol{\nu}_k^T$ is very close to zero for one specific $k \in \{1, \dots, K\}$, then we stop the iteration and only use the first $k - 1$ factors as the final estimates. This means that the users only need to set K_{\max} sufficiently large, and MFAI can automatically find the suitable K without excessive computational costs. The modified algorithm is summarized in Algorithm 4.

An important feature of our MFAI approach is that it can adaptively relate auxiliary

Algorithm 3: Backfitting Algorithm for K -Factor MFAI Model

Data: Main data matrix \mathbf{Y} and auxiliary matrix \mathbf{X}

Result: Estimate of the latent loadings \mathbf{Z} and factors \mathbf{W}

```
1 initialize  $\boldsymbol{\mu}_1, \dots, \boldsymbol{\mu}_K, \boldsymbol{\nu}_1, \dots, \boldsymbol{\nu}_K \leftarrow \text{MFAI\_greedy}(\mathbf{Y}, \mathbf{X})$  ;
2 repeat
3   for  $k = 1, \dots, K$  do
4      $\mathbf{R} \leftarrow \mathbf{Y} - \sum_{k' \neq k} \boldsymbol{\mu}_{k'} \boldsymbol{\nu}_{k'}^T$  ;
5      $\boldsymbol{\mu}_k, a_k^2; \boldsymbol{\nu}_k, b_k^2; \tau_k, \beta_k; F_k(\cdot) \leftarrow \text{MFALS}(\mathbf{R}, \mathbf{X})$  ;
6   end
7 until convergence criterion satisfied;
8 return  $\widehat{\mathbf{Z}} = (\boldsymbol{\mu}_1, \dots, \boldsymbol{\mu}_K), \widehat{\mathbf{W}} = (\boldsymbol{\nu}_1, \dots, \boldsymbol{\nu}_K); a_1^2, \dots, a_K^2, b_1^2, \dots, b_K^2$  ;
9 return  $\tau_1, \dots, \tau_K; \beta_1, \dots, \beta_K$  ;
10 return  $F_1(\cdot), \dots, F_K(\cdot)$ .
```

information with each factor. For example, the mean function $F_k(\cdot)$ and precision β_k are adaptively fitted for the k -th loading without parameter tuning. In contrast, the methods which rely on cross-validation are often limited to tuning two or three parameters due to the unaffordable computational cost of searching in a large parameter space.

Algorithm 4: Greedy Algorithm Automatically Selecting K

Data: Main data matrix \mathbf{Y} and auxiliary matrix \mathbf{X}

Result: Estimate of the latent loadings \mathbf{Z} and factors \mathbf{W}

```
1 set the maximum value of the number of factors  $K_{\max}$  ;
2 set the stop criterion  $sc$  ;
3 for  $k = 1, \dots, K_{\max}$  do
4    $\boldsymbol{\mu}_k, a_k^2; \boldsymbol{\nu}_k, b_k^2; \tau_k, \beta_k; F_k(\cdot) \leftarrow \text{MFAISF}(\mathbf{Y}, \mathbf{X})$  ;
5   if  $\text{Var}(\boldsymbol{\mu}_k \boldsymbol{\nu}_k^T) \cdot \tau_k < sc$  then
6      $K \leftarrow k - 1$  ;
7     break ;
8   end
9    $\mathbf{Y} \leftarrow \mathbf{Y} - \boldsymbol{\mu}_k \boldsymbol{\nu}_k^T$  ;
10 end
11 if  $k = K_{\max}$  then
12    $K \leftarrow K_{\max}$  ;
13 end
14 return  $\widehat{\mathbf{Z}} = (\boldsymbol{\mu}_1, \dots, \boldsymbol{\mu}_K), \widehat{\mathbf{W}} = (\boldsymbol{\nu}_1, \dots, \boldsymbol{\nu}_K); a_1^2, \dots, a_K^2, b_1^2, \dots, b_K^2$  ;
15 return  $\tau_1, \dots, \tau_K; \beta_1, \dots, \beta_K$  ;
16 return  $F_1(\cdot), \dots, F_K(\cdot)$ .
```

3 Numerical Experiments

In this section, we gauge the performance of MFAI in comparison with alternative methods using both simulation and real data analysis. As there are many methods for matrix factorization, we choose the compared methods based on two considerations. First, they are scalable to large-scale datasets. Second, their software are well-maintained and documented. Based on the above criteria, we include EBMF (Wang and Stephens, 2021), CMF (Singh and Gordon, 2008), hardImpute and softImpute (Mazumder et al., 2010; Hastie et al., 2015) in comparison. We summarize these methods with brief descriptions in Table 1. We note that the Bayesian methods (MFAI and EBMF) are self-tuning. The

Method	R package	Brief description
MFAI	mfair	Variational inference, incorporate auxiliary information via gradient boosting machine
EBMF	flashr	Variational inference for a general empirical Bayes matrix factorization model (Wang and Stephens, 2021)
CMF	cmfrec	Main matrix and auxiliary matrix share the same latent factors (Singh and Gordon, 2008; Cortes, 2018)
hardImpute	softImpute	Singular value decomposition (Mazumder et al., 2010)
softImpute	softImpute	Fits a regularized low-rank matrix using a nuclear-norm penalty (Mazumder et al., 2010; Hastie et al., 2015)

Table 1: Overview of the compared methods.

softImpute has a single tuning parameter λ to control the nuclear norm penalty, which is chosen by cross-validation. We apply CMF with default settings. In the spirit of reproducibility, the source code and R scripts used to generate the results of our numerical experiments are made publicly available at <https://github.com/YangLabHKUST/mfair>.

3.1 Simulation Study

3.1.1 Design of the Simulations

The simulation datasets were generated as follows. For all settings, we fixed the number of samples at $N = 1,000$, the number of features at $M = 1,000$, the number of covariates at $C = 3$, and the number of factors at $K = 3$. The auxiliary matrix $\mathbf{X} = [\mathbf{X}_1, \mathbf{X}_2, \mathbf{X}_3] \in \mathbb{R}^{1,000 \times 3}$ was generated from uniform distribution $\mathbf{X}_{nc} \stackrel{i.i.d.}{\sim} \mathcal{U}(-10, 10)$. Then we generated the means of three latent loadings $\mathbf{Z} = [\mathbf{Z}_1, \mathbf{Z}_2, \mathbf{Z}_3] \in \mathbb{R}^{1,000 \times 3}$ via three functions, $F_1(\mathbf{x}) = \frac{1}{2}x_1 - x_2$, $F_2(\mathbf{x}) = \frac{1}{10}x_1^2 - \frac{1}{10}x_2^2 + \frac{1}{5}x_1x_2$, and $F_3(\mathbf{x}) = 5 \sin\left(\frac{1}{100}x_3^3\right)$, respectively. We defined the proportion of variance explained (PVE) by $F_k(\mathbf{X})$ as $\text{PVE}_k = \text{Var}(F_k(\mathbf{X})) / (\text{Var}(F_k(\mathbf{X})) + \beta_k^{-1})$, and controlled $\text{PVE}_k = 0.95$ for $k \in \{1, 2, 3\}$. Note that $F_1(\cdot)$ is linear while $F_2(\cdot)$ and $F_3(\cdot)$ are non-linear. We designed $F_1(\cdot)$, $F_2(\cdot)$, and $F_3(\cdot)$ in these forms to examine whether MAFI could flexibly incorporate auxiliary informa-

tion. The latent factor matrix $\mathbf{W} = [\mathbf{W}_{.1}, \mathbf{W}_{.2}, \mathbf{W}_{.3}] \in \mathbb{R}^{1,000 \times 3}$ was generated from normal distribution $\mathbf{W}_{mk} \stackrel{i.i.d.}{\sim} \mathcal{N}(0, 1)$. With \mathbf{Z} and \mathbf{W} , we obtained true value $\mathbf{Y}^{\text{true}} = \mathbf{Z}\mathbf{W}^T$. At last, we added noises to simulate noisy observation $\mathbf{Y} = \mathbf{Y}^{\text{true}} + \boldsymbol{\epsilon}$, where $\epsilon_{nm} \sim N(0, \tau^{-1})$. Then the PVE by the factors is defined as $\text{PVE} = \text{Var}(\mathbf{Y}^{\text{true}}) / (\text{Var}(\mathbf{Y}^{\text{true}}) + \tau^{-1})$. To mimic the real data with a partially observed main matrix, we randomly masked a subset of entries of \mathbf{Y} , denoted as Ω^{miss} , and considered the remaining entries as observed (i.e., Ω^{obs}). The missing ratio can be computed as $1 - |\Omega^{\text{obs}}| / (NM)$. We specified the number of factors for all methods to be the true value $K = 3$ and repeated the simulations 50 times for each setting.

3.1.2 The Imputation Accuracy

To evaluate the imputation accuracy, we used half of the observed entries in Ω^{obs} as the training set and the remaining entries as the test set, denoted as Ω^{train} and Ω^{test} , respectively. Then, we applied matrix factorization methods to $\mathcal{P}_{\Omega^{\text{train}}}(\mathbf{Y})$ and obtained the output $\hat{\mathbf{Y}}$. The imputation accuracy can be measured by root-mean-square error (RMSE) on the test set Ω^{test}

$$\text{RMSE}(\hat{\mathbf{Y}}, \mathbf{Y}) := \sqrt{\frac{\sum_{(n,m) \in \Omega^{\text{test}}} (\hat{\mathbf{Y}}_{nm} - \mathbf{Y}_{nm})^2}{|\Omega^{\text{test}}|}}. \quad (34)$$

We designed two sets of experiments to test the methods in a wide range of data quality settings. In Experiment 1, we fixed the missing ratio, $1 - |\Omega^{\text{obs}}| / (NM) = 0.5$, and varied PVE to examine the performances of the compared methods under different noise levels. In Experiment 2, we fixed the PVE=0.5 and varied the missing ratio $\in \{0, 0.5, 0.9\}$ to investigate the influence of data sparsity levels.

We summarized the relative RMSE of alternative methods to MFAI in the first row of [Figure 1](#) for Experiment 1. Our MFAI method with backfitting achieved the best accuracy in all parameter settings. When the signal was strong (PVE=0.9), the RMSE of EBMF, hardImpute, and softImpute were slightly lower than MFAI because they could not incorporate auxiliary information to improve matrix factorization. As the PVE decreased, the advantage of MFAI became more evident. Although CMF can also incorporate auxiliary

information, it generally performed poorly in this simulation setting because it can only use linear models to leverage auxiliary information. Furthermore, the parameter tuning of CMF is not adaptive, and its default parameter setting may not be well suitable for the simulation study. Overall, these results suggest that MFAI can effectively leverage the non-linear relationship between auxiliary information and the main matrix to improve imputation performance of matrix factorization at different levels of signal strength.

In Experiment 2, as shown in the second row of [Figure 1](#), the relative performance of alternative methods to MFAI highly depends on the data sparsity. When the main matrix \mathbf{Y} was highly sparse (missing ratio = 0.9), there was little room for improvement if only \mathbf{Y} was available. The MFAI approach achieved greater improvement over other methods by effectively incorporating auxiliary information in a stable manner.

To summarize, MFAI can significantly outperform other approaches when the data quality is poor, such as high sparsity and weak signal. When the data quality is relatively good, it still retains its competitiveness and achieves slight but steady gains. The superior performance of MFAI can be attributed to the following facts: First, MFAI enables a flexible non-linear model to incorporate auxiliary information. Second, our algorithm design seamlessly combines the advantage of the EM algorithm and gradient boosting, making MFAI stable and adaptive.

3.1.3 The Robustness

To exhibit MFAI’s ability to distinguish useful auxiliary covariates from irrelevant ones, we rank the importance of the covariates based on regression trees ([Figure 2](#)), which has been defined in [Section 2.2.3](#). Specifically, we already have the auxiliary matrix $\mathbf{X} \in \mathbb{R}^{1,000 \times 3}$ and the main matrix $\mathbf{Y} \in \mathbb{R}^{1,000 \times 1,000}$ with PVE = 0.5, which were generated as described in [Section 3.1.1](#). These three covariates in \mathbf{X} were known to be important. To introduce irrelevant covariates, we included three covariates by permuting the rows of \mathbf{X} and four additional redundant variables from the uniform distribution $\mathcal{U}(-10, 10)$, denoted as $\mathbf{X}^{\text{pmt}} \in \mathbb{R}^{1,000 \times 3}$ and $\mathbf{X}^{\text{rdd}} \in \mathbb{R}^{1,000 \times 4}$, respectively. At last, we combined the three auxiliary matrices column-wise and got $\mathbf{X}^{\text{all}} = [\mathbf{X}, \mathbf{X}^{\text{pmt}}, \mathbf{X}^{\text{rdd}}] \in \mathbb{R}^{1,000 \times 10}$, in which

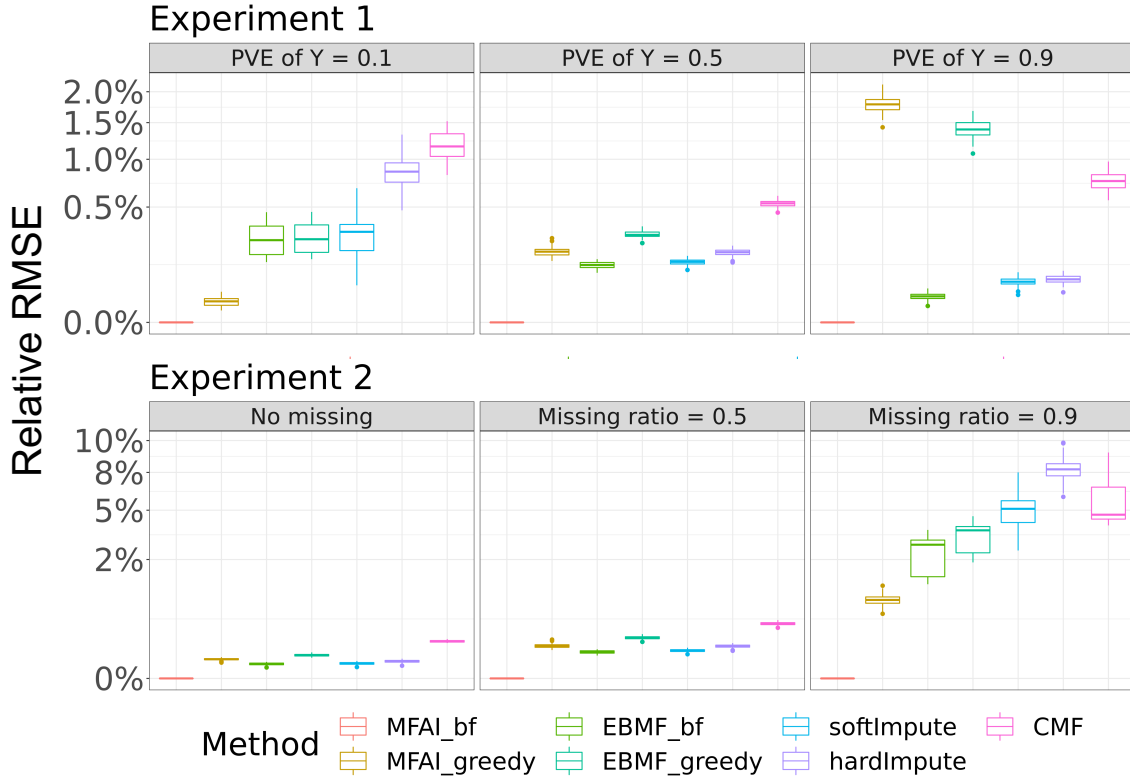


Figure 1: Boxplots comparing the accuracy of different methods. Experiment 1 involves the main matrix \mathbf{Y} that varies from the weak signal (PVE = 0.1, left) to the strong signal (PVE = 0.9, right). Experiment 2 involves the main matrix \mathbf{Y} that varies from low sparsity (missing ratio = 0, left) to high sparsity (missing ratio = 0.9, right). Accuracy is measured by the difference in each method’s RMSE from the MFAI’s RMSE, then divided by the MFAI’s RMSE, with smaller values indicating higher accuracy. The y axis is plotted on the square-root scale to avoid the plots being dominated by methods performed poorly.

the first three columns were useful auxiliary covariates and the remaining seven columns were unimportant. We applied MFAI to \mathbf{Y} and \mathbf{X}^{all} in different situations and visualized the importance scores of all the auxiliary covariates in the first three factors. In the left panel of Figure 2 (first three columns), we masked the main matrix \mathbf{Y} randomly and varied the missing ratio. In the right panel of Figure 2 (next three columns), we fixed the missing ratio of \mathbf{Y} at 0.5, and further masked the auxiliary matrix \mathbf{X}^{all} randomly at the different missing levels. Figure 2 shows that those unimportant auxiliary covariates get

nearly zero importance scores under all data sparsity settings, which indicates that MFAI can effectively distinguish those useful auxiliary covariates, even though the datasets were highly sparse.

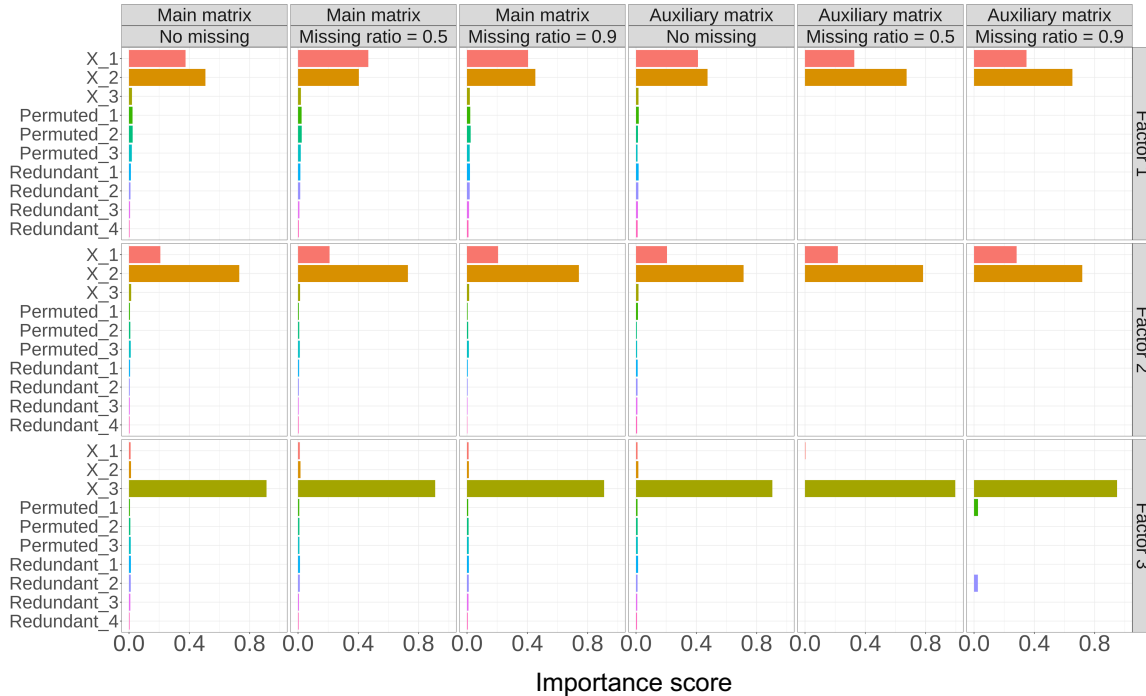


Figure 2: Barplots for the importance scores of the auxiliary covariates in factor 1-3. In the left panel (first three columns), we masked the main matrix \mathbf{Y} randomly and varied from the low sparsity (missing ratio = 0, left) to high sparsity (missing ratio = 0.9, right). In the right panel (next three columns), we first fixed the missing ratio of \mathbf{Y} as 0.5, and further masked the auxiliary matrix \mathbf{X}^{all} randomly and varied from the low sparsity (missing ratio = 0, left) to high sparsity (missing ratio = 0.9, right). The importance scores in each factor have been re-scaled to have a sum of 1. The higher the importance score is, the more the specific covariate contributes to improving the model.

3.1.4 The Computational Efficiency

Finally, we show the computational efficiency of MFAI. We first fixed the sample size $N = 5,000$ and varied the number of features $M \in \{1,000, 2,000, 3,000, 4,000, 5,000\}$ (the left

panel of [Figure 3](#)), and then fixed $M = 5,000$ and varied $N \in \{1,000, 2,000, 3,000, 4,000, 5,000\}$ (the right panel of [Figure 3](#)). To evaluate the computational time of MAFI, we applied

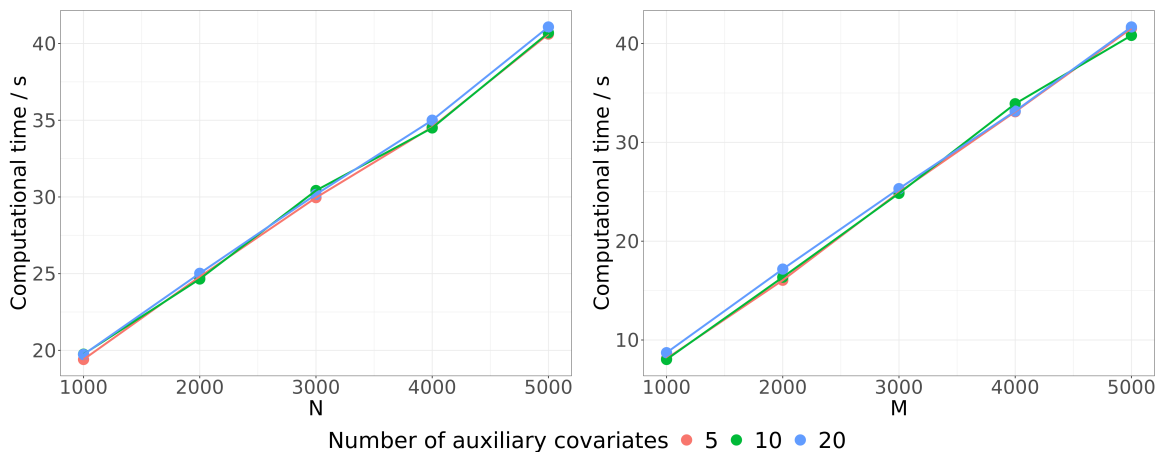


Figure 3: Lineplots for the computational timings against data size. In the left panel, we fixed feature size M and varied sample size N . In the right panel, we fixed sample size N and varied feature size M . Different colors represent the number of auxiliary covariates (i.e., C) used in the model, respectively.

the single-factor MFAI and fixed the number of iteration steps as the same value. As illustrated in [Figure 3](#), the computational complexity of MFAI scales linearly with data size. Furthermore, the experiments were repeated with different numbers of auxiliary covariates (i.e., C), indicated by different colors in [Figure 3](#). Clearly, three lines of varying colors almost coincide, suggesting that the number of auxiliary covariates has little effect on the computational cost.

3.2 Real Data Analysis

3.2.1 Data Description

The two real datasets used in this section are as follows:

MovieLens 100K data is an extensively studied dataset to evaluate the performance of the recommender system ([Harper and Konstan, 2015](#)). The main matrix \mathbf{Y} is a $1,682 \times 943$ matrix of movie-user ratings (0–5 star rating). However, as mentioned in Section

1, most users only rate a small number of movies, making the matrix extremely sparse (missing ratio = 94%), containing about only 100K observed ratings. The auxiliary matrix \mathbf{X} is a $1,682 \times 18$ binary matrix of movie genres, where each row represents a movie, and each column represents a genre. The 18 genres are “Action”, “Adventure”, “Animation”, “Children’s”, “Comedy”, “Crime”, “Documentary”, “Drama”, “Fantasy”, “Film-Noir”, “Horror”, “Musical”, “Mystery”, “Romance”, “Sci-Fi”, “Thriller”, “War”, and “Western”. In order to enhance the matrix factorization performance, we utilize this portion of the data based on the presumption that movies of the same genres should be rated similarly in some sense. We masked a fraction of the observed entries and evaluated the accuracy of different methods in predicting the masked entries.

Human brain gene expression data is a fully observed (i.e., missing ratio = 0) matrix of bulk gene expression (microarray platform) from the human brain transcriptome (HBT) project, where the expression levels of 17,568 genes are measured in 16 brain regions across 15 time periods (Johnson et al., 2009; Kang et al., 2011). We applied the following pre-processing procedure to this dataset. First, periods 1 and 2 correspond to embryonic and early fetal development when most of the 16 brain regions sampled in future periods have not differentiated. Therefore, data in periods 1 and 2 were excluded from our analysis. Second, we focused on analyzing the neocortex areas, including 11 brain regions. Then the main matrix \mathbf{Y} ’s dimension became $886 \times 17,568$, where each row represents a bulk tissue sample, and each column represents a gene. Recent studies have shown that region and age (that is, spatial-temporal dynamics) contribute more to the global differences in gene expression than do other variables: sex, ethnicity, and inter-individual variation (Kang et al., 2011). Hence we extracted the brain region and time period information for each sample from the raw data as auxiliary information. The auxiliary information \mathbf{X} here is represented as an 886×2 data frame. The first column is a vector of factor types indicating which region the sample belongs to. The second column is a vector containing the time period information. We provide more detailed data information (neocortex areas and time periods introduction) in Appendices Section B.1.

Both Bayesian methods MFAI and EBMF can automatically estimate K . For MFAI, we

set $K_{\max} = 20$ for MovieLens 100K data and $K_{\max} = 150$ for human brain gene expression data which are sufficiently large. For softImpute, hardImpute, and CMF, we specified K based on the values inferred by MFAI. As for the other parameters, we applied softImpute with λ chosen by cross-validation and CMF with default settings. We first compared the imputation accuracy in terms of the RMSE. Then we showed that MFAI provided more comprehensive insights into these two real datasets than the compared methods by investigating the inferred factors and loadings.

3.2.2 The Imputation Accuracy

In this section, we examined the imputation performance of compared methods (Figure 4). First, we randomly split the observed entries Ω^{obs} into a training set Ω^{train} and a test set Ω^{test} . Then we applied matrix factorization methods to the training data and predicted the entries in the held-out set. The imputation accuracy of the held-out entries was measured by RMSE (34). We considered different values of the “training ratio”, denoted as training ratio = $|\Omega^{\text{train}}|/|\Omega^{\text{obs}}|$. For human brain gene expression data, $\Omega^{\text{obs}} = \Omega$ since it is fully observed. We repeated the experiments 50 times for each setting of the training ratio. MFAI used only around two minutes to analyze MovieLens 100K data with inferred $K = 9$ and around 150 minutes to analyze human brain gene expression data with inferred $K = 95$, using 4 CPU cores of Intel(R) Xeon(R) Gold 6230N CPU @ 2.30GHz processor on a Linux computing platform. By contrast, EBMF, another Bayesian method that cannot incorporate auxiliary information, used around one minute to analyze MovieLens 100K data and around 130 minutes to analyze human brain gene expression data using the same computing resources, suggesting that MFAI can leverage auxiliary information with only minor computational overhead.

We summarized the RMSE across 50 times experiments in Figure 4. For MovieLens 100K data MFAI and CMF outperformed other methods by incorporating the movie genre information, suggesting the movie genre provides useful information to predict user ratings. MFAI gained greater improvement from the movie genre information than CMF because the gradient-boosted tree offers a more flexible structure than the linear model in CMF to

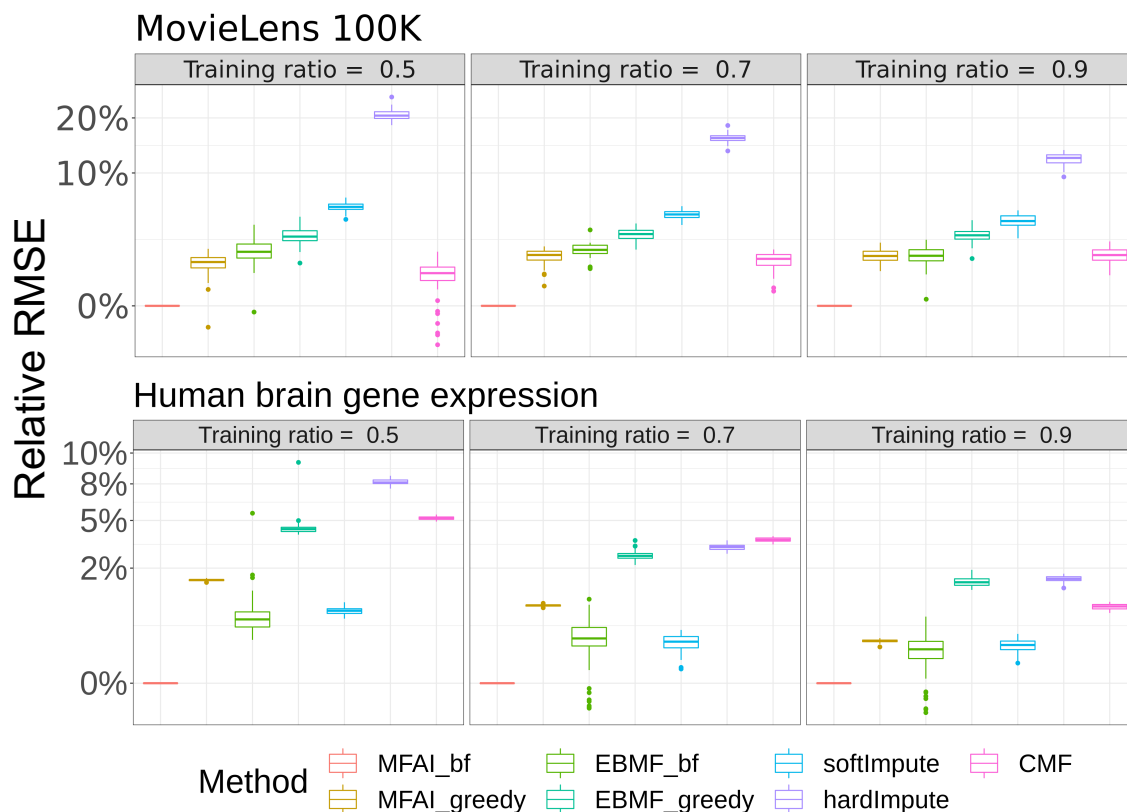


Figure 4: Boxplots comparing the accuracy of different methods in imputing missing entries. These two sets of experiments involve the main matrix \mathbf{Y} that varies from rare information (training ratio = 0.5, left) to rich information (training ratio = 0.9, right). Accuracy is measured by the difference in each method’s RMSE from the MFAI’s RMSE, then divided by the MFAI’s RMSE, with smaller values indicating higher accuracy. The y axis is plotted on the square-root scale to avoid the plots being dominated by methods performed poorly.

model the connection between the loading and genre of a movie. For the human brain gene expression data, the auxiliary information comes from two different sources—brain regions and time periods, where regions are represented as categorical variables and time periods are represented as numerical variables. MFAI also achieved the best performance among the compared methods because the tree structure in MFAI is very good at handling mixed data types (i.e., categorical and numerical variables). In contrast, CMF did not perform

well in this dataset, which may be attributed to the fact that the linear models are often not good at handling mixed data types and capturing possible spatial-temporal interaction effects in the gene expression data. These evidence suggests that MFAI can effectively leverage auxiliary information to improve the imputation accuracy in the highly sparse dataset by taking the advantage of the gradient boosted tree structure.

3.2.3 Enrichment of Movie Genres in MovieLens 100K Data Analysis

In this section, we use MovieLens 100K data to illustrate the ability of MFAI to identify important variables in auxiliary information through decision trees, which allows us to gain a deeper understanding of the connection between the main matrix and the auxiliary information (Figure 5). As a negative control, we constructed a permuted movie genre matrix $\mathbf{X}^{\text{pmt}} \in \mathbb{R}^{1,682 \times 18}$, where the c -th column $\mathbf{X}_{\cdot c}^{\text{pmt}}$ was obtained by permuting the entries of $\mathbf{X}_{\cdot c}$ for $c = 1, \dots, 18$. We applied MFAI to the whole MovieLens 100K data with three different auxiliary matrices \mathbf{X} , \mathbf{X}^{pmt} , and $\mathbf{X}^{\text{both}} = [\mathbf{X}, \mathbf{X}^{\text{pmt}}] \in \mathbb{R}^{1,682 \times 36}$. In each experiment, we initialized the model parameters with the same values and computed the importance scores of auxiliary covariates.

Figure 5 visualizes the importance scores of auxiliary covariates in the top three factors. The top left panel shows the importance scores obtained with \mathbf{X} , which indicates the relevance of true movie genres to user ratings. We can see that in factor 1, “Drama” is the leading genre while “Children’s”, “Comedy”, “Film-Noir”, “Horror”, and “War” also contribute to this factor; “Action” and “Children’s” are two major genres in factor 2; “Children’s”, “Comedy”, and “Musical” exert influence in factor 3. When using the permuted matrix \mathbf{X}^{pmt} as input (bottom left panel of Figure 5), MFAI correctly assigned low importance scores to all permuted genres, suggesting that MFAI avoids incorporating irrelevant auxiliary information. Finally, in the presence of both true and permuted movie genres (right panel of Figure 5), MFAI successfully distinguished the useful movie genres from irrelevant ones. By comparing the left panels and the right panel of Figure 5), we can observe that the importance scores obtained using \mathbf{X}^{both} are highly consistent with those obtained using \mathbf{X} and \mathbf{X}^{pmt} as separate inputs, indicating the stability and robustness of

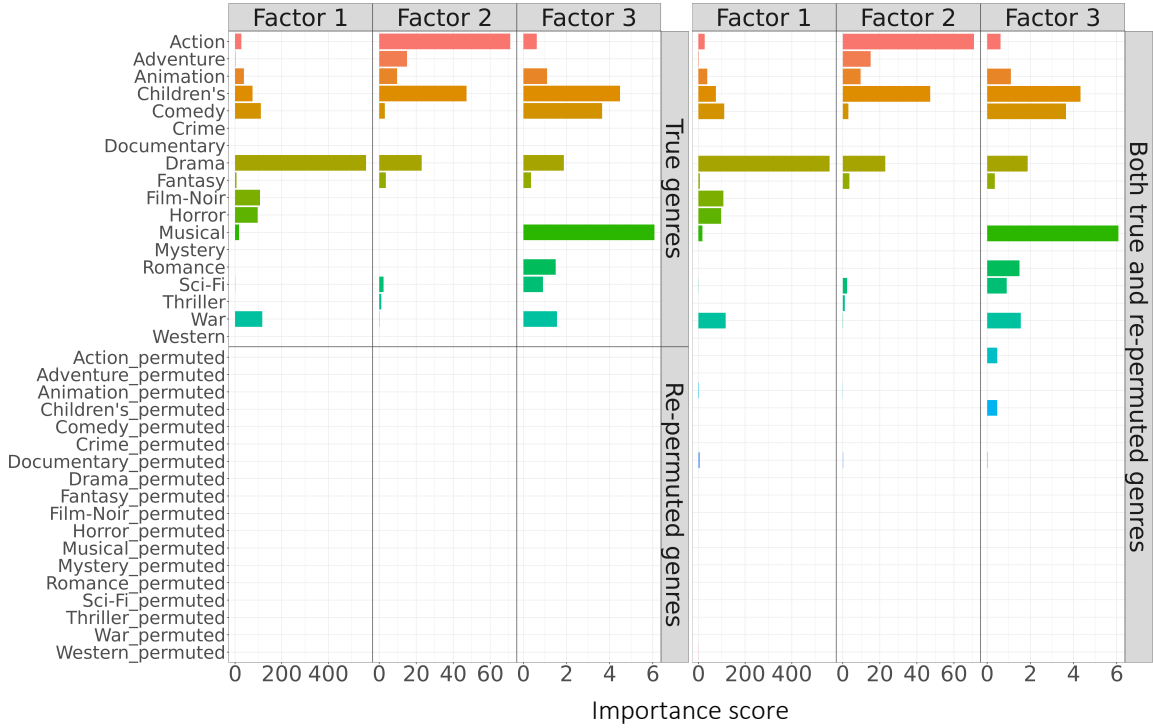


Figure 5: Barplots for the importance scores of the auxiliary covariates in the top 3 factors of MovieLens 100K data. In the top left panel, we only used the true movie genre information \mathbf{X} as the input. In the bottom left panel, we only used the re-permuted movie genre information \mathbf{X}^{pmt} as the input. In the right panel, we used both the true and re-permuted movie genre information \mathbf{X}^{pmt} as the input. The higher the importance score is, the more a specific movie genre contributes to improving the model.

MFAI.

3.2.4 Spatial and Temporal Dynamics of Gene Regulation Among Tissues

The spatial and temporal patterns of gene regulation during brain development have attracted a great deal of attention in the neuroscience community. The availability of gene expression profiles collected from multiple brain regions and time periods provides an unprecedented chance to characterize human brain development. Despite the availability of rich resources, turning such a wealth of data into knowledge about the brain requires

much modeling effort. The aforementioned human brain gene expression data has been analyzed by several statistical methods, e.g., [Lin et al. \(2015\)](#) modeled spatial and temporal patterns with Markov random field (MRF), [Lin et al. \(2017\)](#) proposed a Bayesian neighborhood selection method to estimate the network structure, and [Liu et al. \(2022\)](#) developed a low-rank tensor decomposition method to capture spatial and temporal effects simultaneously. By modeling the relationship between the spatial-temporal information with the gene expression matrix via non-linear functions $F_k(\cdot)$, MFAI can offer biological insights into the heterogeneity in temporal dynamics across different brain regions and the evolution of spatial patterns over multiple time periods. Following [Hawrylycz et al. \(2015\)](#), we selected genes with consistent spatial patterns across individuals using the concept of differential stability (DS), which was defined as the tendency for a gene to exhibit reproducible differential expression relationships across brain structures (see more details in Appendices Section B.2). As inputs of MFAI, we included 2,000 genes with the highest DS, resulting in the new main matrix $\mathbf{Y} \in \mathbb{R}^{886 \times 2,000}$, and used the same auxiliary $\mathbf{X} \in \mathbb{R}^{886 \times 2}$ with spatial and temporal information.

To gain insights, the dynamic patterns of the top three factors across different neocortex areas and time periods, represented by $\{F_1(\cdot), F_2(\cdot), F_3(\cdot)\}$, are given in [Figure 6 A](#). Each factor has been normalized to have the l_2 -norm equal one. It is obvious that fitted functions $\{F_1(\cdot), F_2(\cdot), F_3(\cdot)\}$ not only capture the non-linearity across different time periods but also implicate spatial-temporal interactions. As such MFAI fully made use of the auxiliary information. In contrast, methods only considering simple linear relationships may cause information loss. Overall, all three factors show stronger temporal differences, compared to spatial differences within the neocortex areas. The temporal trajectories of all three factors show clear signs of prenatal development (from Period 3 to Period 7). From infancy (Period 8 and afterward), Factor 2 exhibits increasing influence while Factor 3 exhibits decreasing influence in magnitude. Then all three factors keep steady levels until late adulthood. All the non-V1C neocortex areas show particularly pronounced correlations and consistency during development. Factor 1 and Factor 3 in V1C showed distinctive signals throughout development and adulthood, compared to other neocortex areas.

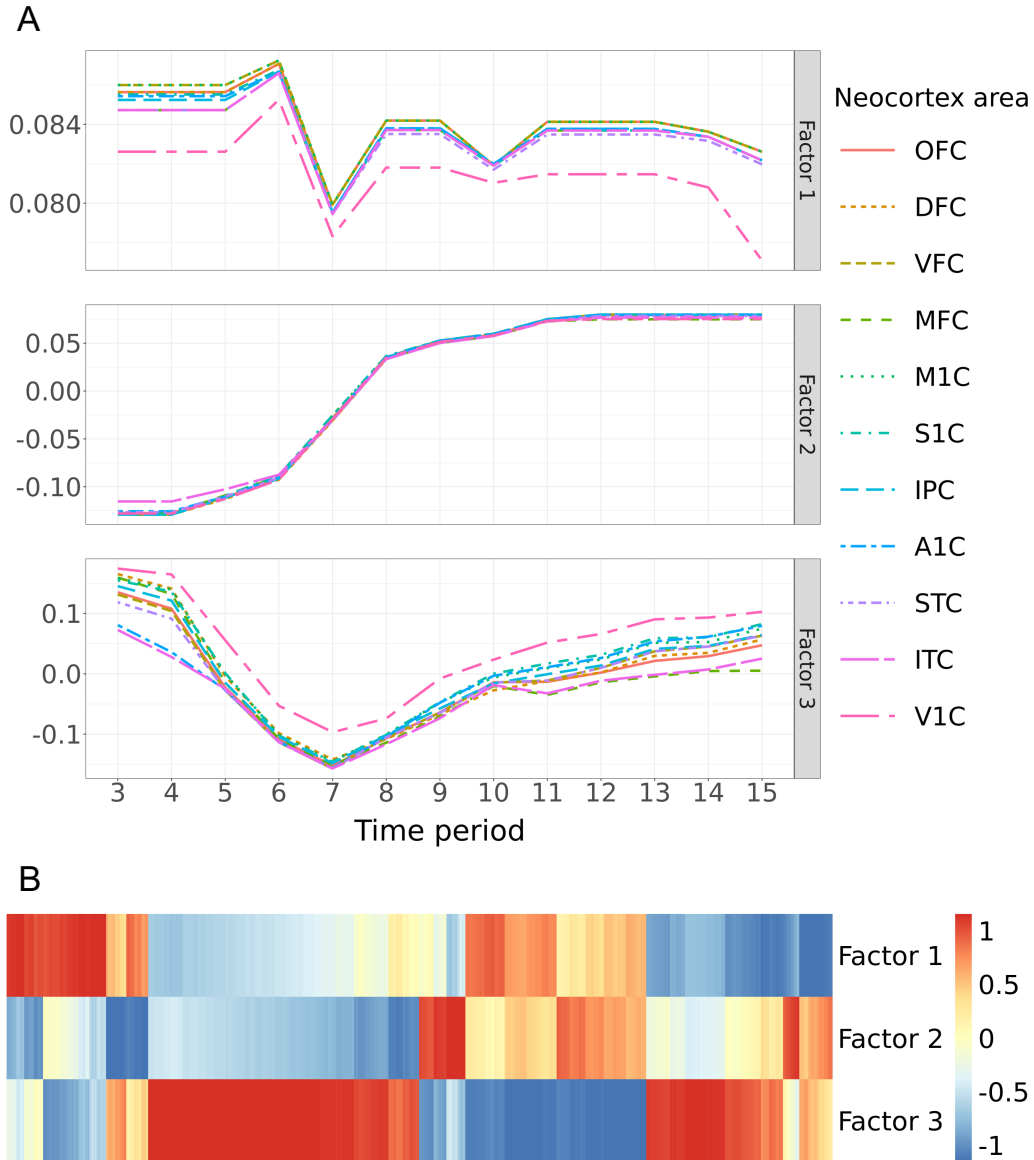


Figure 6: Spatial-temporal dynamic patterns in Factor 1 - 3. In Figure A, we visualize the loading levels across different neocortex areas and time periods of the top 3 factors (i.e., $\{F_1(\cdot), F_2(\cdot), F_3(\cdot)\}$). The loading levels have been normalized before visualization. Figure B is the heatmap of the corresponding top 3 factors (i.e., $\{\mathbf{W}_{.1}, \mathbf{W}_{.2}, \mathbf{W}_{.3}\}$), where each column represents a gene. The gene factors have been normalized before visualization.

Figure 6 B is the heatmap of the top three inferred gene factors $[\mathbf{W}_1, \mathbf{W}_2, \mathbf{W}_3] \in \mathbb{R}^{2,000 \times 3}$. To better understand these three factors, we conducted the gene set enrichment analysis based on Gene Ontology (<http://geneontology.org/>) for each factor. Specifically, we first calculated the relative weight of the k -th factor for the m -th gene by $|\mathbf{W}_{mk}| / \sum_{k'=1}^3 |\mathbf{W}_{mk'}|$, where $\mathbf{W}_m \in \mathbb{R}^{3 \times 1}$ is the m -th row of gene factors, and then selected the top 300 weighted genes in each factor to form the gene sets. The enriched biological processes with corresponding P -values after Bonferroni correction are summarized in Table 2. Factor 1 relates with the axon and neuron development, consistent with

	Biological process	P -value with Bonferroni correction
Factor 1	Axon development	1.97E-02
	Neuron development	1.82E-03
	Neuron differentiation	8.03E-05
Factor 2	Regulation of biological quality	2.25E-10
	Potassium ion transmembrane transport	6.25E-05
	Regulation of transport	2.84E-07
	Signaling	5.35E-05
	Cell communication	1.02E-04
Factor 3	Regulation of cell junction assembly	4.04E-03
	Cell adhesion	8.07E-04
	Cell junction assembly	3.84E-04
	Nervous system development	5.58E-05

Table 2: Gene enrichment analysis on Factor 1-3.

its status as the leading factor in the neocortex and relatively high signal level across all time periods as shown in Figure 6 A. Factor 2 is enriched in signaling (Luebke and Rosene, 2003; Luebke et al., 2004) and cell communication (López-Otín et al., 2013), which are aging-related processes. It is also known that aging induces specific changes in individual ATPases according to their subsynaptic localization (de Lores Arnaiz and Ordieres, 2014). For example, Na^+ , K^+ -ATPase activity in hippocampus tends to decrease by age (Kinjo

et al., 2007), consistent with the temporal pattern of Factor 2 shown in Figure 6 A. Combining Figure 6 A and Figure 6 B, the enrichment of Factor 2 in the ion transport provides evidence that the interstitial ion is a key regulator of state-dependent neural activity (Rasmussen et al., 2020). Factor 3 is mainly enriched in cell junctions which play an important role during the development of the mammalian brain (Montoro and Yuste, 2004). In the neocortex, gap junctions are already expressed at very early stages of development and are involved in many processes like neurogenesis, migration, and synapse formation (Sutor and Hagerty, 2005). In the mammalian central nervous system (CNS), coupling of neurons by gap junctions (i.e., electrical synapses) and the expression of the neuronal gap junction protein, connexin 36 (Cx36), transiently increases during early postnatal development, then subsequently declines and remains low in the adulthood, confined to specific subsets of neurons (Belousov and Fontes, 2013). This trend is highly consistent with the temporal pattern of Factor 3 shown in Figure 6 A, reaching a brief high magnitude around birth and quickly falling back.

4 Conclusion

The auxiliary information is particularly useful to improve matrix factorization when the observed matrix is noisy and sparse. Despite the massive availability of auxiliary information in real applications, existing methods largely rely on linear models to connect auxiliary covariates with the main matrix and hence lead to sub-optimal performance.

In this paper, we propose a scalable matrix factorization approach named MFAI to leverage auxiliary information. By integrating the gradient boosted trees with probabilistic matrix factorization, MFAI enables nonlinear modeling of auxiliary covariates and allows the model parameters to be automatically estimated under the empirical Bayes framework, making MFAI adaptive to the complicated connections between the main matrix and auxiliary information. Besides, MFAI naturally inherits several salient features of gradient boosted trees, such as the robustness to irrelevant features, immunity to missing values in predictors, and the ability to distinguish useful covariates in the auxiliary information. Under the variational assumption, we developed an efficient algorithm that can simultaneously

estimate the number of latent factors and infer the structure. With our innovations in the model and algorithm designs, our *mfair* software is fast, stable, and scalable to large-scale datasets. Through comprehensive simulation studies, we showed that MFAI is statistically accurate and computationally efficient, especially in the scenario of high sparsity and weak signal strength. We applied MFAI to two real datasets, including one human brain gene expression dataset, and showed that MFAI not only improves the imputation accuracy but also yields biological insights into spatiotemporal gene regulation patterns in the human brain.

Acknowledgements

This work is supported in part by Hong Kong Research Grant Council Grants 16307818, 16301419, 16308120, and 16307221; Hong Kong Innovation and Technology Fund Grant PRP/029/19FX; The Hong Kong University of Science and Technology Startup Grants R9405 and Z0428 from the Big Data Institute; City University of Hong Kong Startup Grant 7200746. The computational task for this work was performed by using the X-GPU cluster supported by the Research Grants Council Collaborative Research Fund Grant C6021-19EF.

SUPPLEMENTARY MATERIAL

Appendices: The online appendices containing Section A with details of the method and Section B with additional description of the human brain gene expression data (Appendices.pdf, PDF file).

R package for MFAI: The R-package *mfair* containing the functions used in fitting MFAI (mfair.zip, ZIP file).

Compared Methods:

EBMF: <https://github.com/stephenslab/flashr>

CMF: <https://cran.r-project.org/package=cmfrec>

softImpute: <https://cran.r-project.org/package=softImpute>

Appendices to “MFAI: A Scalable Bayesian Matrix Factorization Approach to Leveraging Auxiliary Information”

A Fitting the Single-Factor MFAI Model

Given the main data matrix $\mathbf{Y} \in \mathbb{R}^{N \times M}$ of N samples and M features, and the auxiliary matrix $\mathbf{X} \in \mathbb{R}^{N \times C}$ of N samples and C covariates, we consider the following single-factor matrix factorization problem

$$\begin{aligned} \mathbf{Y} &= \mathbf{z}\mathbf{w}^T + \boldsymbol{\epsilon}, \\ \mathbf{z} &\sim \mathcal{N}_N(F(\mathbf{X}), \beta^{-1}\mathbf{I}_N), \\ \mathbf{w} &\sim \mathcal{N}_M(0, \mathbf{I}_M), \\ \epsilon_{nm} &\sim \mathcal{N}(0, \tau^{-1}), \quad n = 1, \dots, N \text{ and } m = 1, \dots, M, \end{aligned} \tag{35}$$

where $\mathbf{z} \in \mathbb{R}^{N \times 1}$ is the latent loading, $\mathbf{w} \in \mathbb{R}^{M \times 1}$ is the latent factor, $\boldsymbol{\epsilon} \in \mathbb{R}^{N \times M}$ is a matrix of residual error terms, $F : \mathbb{R}^C \rightarrow \mathbb{R}$ is the unknown function, $F(\mathbf{X}) \in \mathbb{R}^{N \times 1}$ denotes $(F(\mathbf{X}_1), \dots, F(\mathbf{X}_N))^T$, $\mathbf{X}_n = (\mathbf{X}_{n1}, \dots, \mathbf{X}_{nC})^T \in \mathbb{R}^{C \times 1}$ is the n -th row of \mathbf{X} containing auxiliary information for the n -th row entity for $n = 1, \dots, N$, and β and τ are two precision parameters. Then the joint probabilistic model becomes

$$\Pr(\mathbf{Y}, \mathbf{z}, \mathbf{w} \mid \boldsymbol{\theta}, F(\cdot)) = \Pr(\mathbf{Y} \mid \mathbf{z}, \mathbf{w}; \tau) \Pr(\mathbf{z} \mid \beta, F(\cdot)) \Pr(\mathbf{w}), \tag{36}$$

where $\boldsymbol{\theta} = \{\tau, \beta\}$ is the collection of model parameters. The goal is to estimate $\boldsymbol{\theta}$ and $F(\cdot)$ by optimizing the log marginal likelihood

$$\begin{aligned} (\hat{\boldsymbol{\theta}}, \hat{F}(\cdot)) &= \arg \max_{\boldsymbol{\theta}, F(\cdot)} \log \Pr(\mathbf{Y} \mid \boldsymbol{\theta}, F(\cdot)) \\ &= \arg \max_{\boldsymbol{\theta}, F(\cdot)} \log \int \Pr(\mathbf{Y}, \mathbf{z}, \mathbf{w} \mid \boldsymbol{\theta}, F(\cdot)) \, d\mathbf{z} \, d\mathbf{w}. \end{aligned} \tag{37}$$

The posterior probability of \mathbf{z} and \mathbf{w} is given as

$$\Pr(\mathbf{z}, \mathbf{w} \mid \mathbf{Y}; \hat{\boldsymbol{\theta}}, \hat{F}(\cdot)) = \frac{\Pr(\mathbf{Y}, \mathbf{z}, \mathbf{w} \mid \hat{\boldsymbol{\theta}}, \hat{F}(\cdot))}{\Pr(\mathbf{Y} \mid \hat{\boldsymbol{\theta}}, \hat{F}(\cdot))}. \tag{38}$$

A.1 Approximate Bayesian Inference

The Bayesian inference using (37) and (38) is intractable since the marginal likelihood $\Pr(\mathbf{Y} \mid \boldsymbol{\theta}, F(\cdot))$ cannot be computed by marginalizing all latent variables. To tackle the Bayesian inference problem, here we propose a variational expectation-maximization (EM) algorithm (Bishop, 2006; Blei et al., 2017) to perform approximate Bayesian inference. To apply variational approximation, we first define $q(\mathbf{z}, \mathbf{w})$ as an approximated distribution of posterior $\Pr(\mathbf{z}, \mathbf{w} \mid \mathbf{Y}; \boldsymbol{\theta}, F(\cdot))$. Then the logarithm of the marginal likelihood is

$$\begin{aligned}
 \log \Pr(\mathbf{Y} \mid \boldsymbol{\theta}, F(\cdot)) &= \log \int \Pr(\mathbf{Y}, \mathbf{z}, \mathbf{w} \mid \boldsymbol{\theta}, F(\cdot)) \, d\mathbf{z} \, d\mathbf{w} \\
 &= \log \int q(\mathbf{z}, \mathbf{w}) \frac{\Pr(\mathbf{Y}, \mathbf{z}, \mathbf{w} \mid \boldsymbol{\theta}, F(\cdot))}{q(\mathbf{z}, \mathbf{w})} \, d\mathbf{z} \, d\mathbf{w} \\
 &\geq \int q(\mathbf{z}, \mathbf{w}) \log \frac{\Pr(\mathbf{Y}, \mathbf{z}, \mathbf{w} \mid \boldsymbol{\theta}, F(\cdot))}{q(\mathbf{z}, \mathbf{w})} \, d\mathbf{z} \, d\mathbf{w} \tag{39} \\
 &= \mathbb{E}_q [\log \Pr(\mathbf{Y}, \mathbf{z}, \mathbf{w} \mid \boldsymbol{\theta}, F(\cdot))] - \mathbb{E}_q [\log q(\mathbf{z}, \mathbf{w})] \\
 &\equiv \text{ELBO}(q),
 \end{aligned}$$

where we have adopted Jensen’s inequality to obtain the evidence lower bound (ELBO). The equality holds if and only if $q(\mathbf{z}, \mathbf{w})$ is the exact posterior $\Pr(\mathbf{z}, \mathbf{w} \mid \mathbf{Y}; \boldsymbol{\theta}, F(\cdot))$. Instead of maximizing the logarithm of the marginal likelihood, we can iteratively maximize the ELBO with respect to the variational approximate posterior q , the model parameters $\boldsymbol{\theta}$, and the function $F(\cdot)$

$$\left(\widehat{q}; \widehat{\boldsymbol{\theta}}, \widehat{F}(\cdot) \right) = \arg \max_{q; \boldsymbol{\theta}, F(\cdot)} \text{ELBO}(q; \boldsymbol{\theta}, F(\cdot)). \tag{40}$$

Using the terminology in the EM algorithm, maximization of ELBO with respect to q is known as the E-step, and maximization of ELBO with respect to $\boldsymbol{\theta}$ and $F(\cdot)$ is known as the M-step.

A.1.1 E-step

In the E-step, we aim to find the optimal solution for the approximate posterior with the current estimate for model parameters $\boldsymbol{\theta}$ and function $F(\cdot)$, i.e., we treat $\boldsymbol{\theta}$ and $F(\cdot)$ are

fixed. Then the complete-data log-likelihood is given as

$$\begin{aligned}
\log \Pr(\mathbf{Y}, \mathbf{z}, \mathbf{w} \mid \tau, \beta; F(\cdot)) &= \log \Pr(\mathbf{Y} \mid \mathbf{z}, \mathbf{w}; \tau) + \log \Pr(\mathbf{z} \mid \beta; F(\cdot)) + \log \Pr(\mathbf{w}) \\
&= -\frac{NM}{2} \log(2\pi) + \frac{NM}{2} \log \tau - \frac{\tau}{2} \|\mathbf{Y} - \mathbf{z}\mathbf{w}^T\|_F^2 \\
&\quad - \frac{N}{2} \log(2\pi) + \frac{N}{2} \log \beta - \frac{\beta}{2} \|\mathbf{z} - F(\mathbf{X})\|_2^2 \\
&\quad - \frac{M}{2} \log(2\pi) - \frac{1}{2} \|\mathbf{w}\|_2^2,
\end{aligned} \tag{41}$$

where $\|\cdot\|_F$ for a matrix denotes the Frobenius norm and $\|\cdot\|_2$ for a vector denotes the Euclidean norm. The next step is to maximize ELBO instead of working with the marginal likelihood directly. As in the main text, we use the following factorized distribution to approximate the true posterior

$$q(\mathbf{z}, \mathbf{w}) = q(\mathbf{z})q(\mathbf{w}). \tag{42}$$

Amongst all distributions $q(\mathbf{z}, \mathbf{w})$ having the form (42), we now seek that distribution for which the ELBO (q) is largest. To achieve this, we make a variational optimization of ELBO (q) with respect to each of the factors $q(\mathbf{z})$ and $q(\mathbf{w})$ in turn. For simplicity, we ignore the notation of the model parameters $\boldsymbol{\theta}$ and function $F(\cdot)$ in this part. We first keep the $q(\mathbf{w})$ fixed, then the ELBO can be written in the following form

$$\begin{aligned}
\text{ELBO}(q) &= \mathbb{E}_{q(\mathbf{z})} [\mathbb{E}_{q(\mathbf{w})} [\log \Pr(\mathbf{Y}, \mathbf{z}, \mathbf{w})] - \log q(\mathbf{z})] + \text{const} \\
&= \int q(\mathbf{z}) \frac{\log \widetilde{\Pr}(\mathbf{Y}, \mathbf{z})}{\log q(\mathbf{z})} d\mathbf{z} + \text{const},
\end{aligned} \tag{43}$$

where we have defined a new distribution $\log \widetilde{\Pr}(\mathbf{Y}, \mathbf{z})$ by the relation

$$\log \widetilde{\Pr}(\mathbf{Y}, \mathbf{z}) = \mathbb{E}_{q(\mathbf{w})} [\log \Pr(\mathbf{Y}, \mathbf{z}, \mathbf{w})] + \text{const}. \tag{44}$$

By recognizing that (43) is a negative Kullback–Leibler (KL) divergence between $q(\mathbf{z})$ and $\widetilde{\Pr}(\mathbf{Y}, \mathbf{z})$, it's clear that the ELBO achieves maximum value when $q(\mathbf{z}) = \widetilde{\Pr}(\mathbf{Y}, \mathbf{z})$. Hence

we can obtain the optimal solution for $q(\mathbf{z})$ by

$$\begin{aligned}
& \log q(\mathbf{z}) \\
&= \mathbb{E}_{q(\mathbf{w})} [\log \Pr(\mathbf{Y}, \mathbf{z}, \mathbf{w})] + \text{const} \\
&= \mathbb{E}_{q(\mathbf{w})} \left[-\frac{\tau}{2} \|\mathbf{Y} - \mathbf{z}\mathbf{w}^T\|_F^2 \right] - \frac{\beta}{2} \|\mathbf{z} - F(\mathbf{X})\|_2^2 + \text{const} \\
&= -\frac{\tau}{2} \sum_{m=1}^M \mathbb{E}_{q(\mathbf{w})} \left[(\mathbf{Y}_{.m} - \mathbf{w}_m \mathbf{z})^T (\mathbf{Y}_{.m} - \mathbf{w}_m \mathbf{z}) \right] - \frac{\beta}{2} (\mathbf{z} - F(\mathbf{X}))^T (\mathbf{z} - F(\mathbf{X})) + \text{const} \\
&= -\frac{1}{2} \mathbf{z}^T \text{diag}(\beta + \tau \mathbb{E}_{q(\mathbf{w})} [\|\mathbf{w}\|_2^2])_N \mathbf{z} + \mathbf{z}^T (\beta F(\mathbf{X}) + \tau \mathbf{Y} \mathbb{E}_{q(\mathbf{w})} [\mathbf{w}]) + \text{const},
\end{aligned} \tag{45}$$

where $\text{diag}(\beta + \tau \mathbb{E}_{q(\mathbf{w})} [\|\mathbf{w}\|_2^2])_N = (\beta + \tau \mathbb{E}_{q(\mathbf{w})} [\|\mathbf{w}\|_2^2]) \mathbf{I}_N \in \mathbb{R}^{N \times N}$ is a diagonal matrix. Then we fix $q(\mathbf{z})$ and optimize ELBO(q) with respect to $q(\mathbf{w})$. Similarly, the ELBO can be written as

$$\begin{aligned}
\text{ELBO}(q) &= \mathbb{E}_{q(\mathbf{w})} [\mathbb{E}_{q(\mathbf{z})} [\log \Pr(\mathbf{Y}, \mathbf{z}, \mathbf{w})] - \log q(\mathbf{w})] + \text{const} \\
&= \int q(\mathbf{w}) \frac{\log \widetilde{\Pr}(\mathbf{Y}, \mathbf{w})}{\log q(\mathbf{w})} d\mathbf{w} + \text{const},
\end{aligned} \tag{46}$$

where

$$\log \widetilde{\Pr}(\mathbf{Y}, \mathbf{w}) = \mathbb{E}_{q(\mathbf{z})} [\log \Pr(\mathbf{Y}, \mathbf{z}, \mathbf{w})] + \text{const}. \tag{47}$$

And the optimal solution for $q(\mathbf{w})$ is given by

$$\begin{aligned}
& \log q(\mathbf{w}) \\
&= \mathbb{E}_{q(\mathbf{z})} [\log \Pr(\mathbf{Y}, \mathbf{z}, \mathbf{w})] + \text{const} \\
&= \mathbb{E}_{q(\mathbf{z})} \left[-\frac{\tau}{2} \|\mathbf{Y} - \mathbf{z}\mathbf{w}^T\|_F^2 \right] - \frac{1}{2} \|\mathbf{w}\|_2^2 + \text{const} \\
&= -\frac{\tau}{2} \sum_{n=1}^N \mathbb{E}_{q(\mathbf{z})} \left[(\mathbf{Y}_{n.} - \mathbf{z}_n \mathbf{w})^T (\mathbf{Y}_{n.} - \mathbf{z}_n \mathbf{w}) \right] - \frac{1}{2} \mathbf{w}^T \mathbf{w} + \text{const} \\
&= -\frac{1}{2} \mathbf{w}^T \text{diag}(1 + \tau \mathbb{E}_{q(\mathbf{z})} [\|\mathbf{z}\|_2^2])_M \mathbf{w} + \mathbf{w}^T (\tau \mathbf{Y}^T \mathbb{E}_{q(\mathbf{z})} [\mathbf{z}]) + \text{const},
\end{aligned} \tag{48}$$

where $\text{diag}(1 + \tau \mathbb{E}_{q(\mathbf{z})} [\|\mathbf{z}\|_2^2])_M = (1 + \tau \mathbb{E}_{q(\mathbf{z})} [\|\mathbf{z}\|_2^2]) \mathbf{I}_M \in \mathbb{R}^{M \times M}$ is a diagonal matrix. The quadratic forms (45) and (48) indicate that both \mathbf{z} and \mathbf{w} follow Gaussian distribution

$$q(\mathbf{z}) = \mathcal{N}_N(\mathbf{z} \mid \boldsymbol{\mu}, \mathbf{A}), \quad q(\mathbf{w}) = \mathcal{N}_M(\mathbf{w} \mid \boldsymbol{\nu}, \mathbf{B}), \tag{49}$$

where $\boldsymbol{\mu} \in \mathbb{R}^{N \times 1}$ and $\boldsymbol{\nu} \in \mathbb{R}^{M \times 1}$ are posterior mean vectors and $\mathbf{A} \in \mathbb{R}^{N \times N}$ and $\mathbf{B} \in \mathbb{R}^{M \times M}$ are covariance matrices

$$\begin{aligned}\mathbf{A} &= \text{diag}(a^2)_N, \quad \frac{1}{a^2} \boldsymbol{\mu} = \beta F(\mathbf{X}) + \tau \mathbf{Y} \boldsymbol{\nu}, \\ \mathbf{B} &= \text{diag}(b^2)_M, \quad \frac{1}{b^2} \boldsymbol{\nu} = \tau \mathbf{Y}^T \boldsymbol{\mu},\end{aligned}\tag{50}$$

and

$$a^2 = \frac{1}{\beta + \tau (\|\boldsymbol{\nu}\|_2^2 + Mb^2)}, \quad b^2 = \frac{1}{1 + \tau (\|\boldsymbol{\mu}\|_2^2 + Na^2)}.\tag{51}$$

A.1.2 M-step

In the M-step, we turn to fix the variational approximate posterior $q(\mathbf{z}, \mathbf{w})$ and maximize the ELBO with respect to $\boldsymbol{\theta}$ and $F(\cdot)$. With (49), the ELBO is given by

$$\begin{aligned}& \text{ELBO}(q; \tau, \beta; F(\cdot)) \\ &= \mathbb{E}_q[\log \Pr(\mathbf{Y}, \mathbf{z}, \mathbf{w})] - \mathbb{E}_q[\log q(\mathbf{z}, \mathbf{w})] \\ &= -\frac{NM}{2} \log(2\pi) + \frac{NM}{2} \log \tau \\ &\quad - \frac{\tau}{2} \left(\|\mathbf{Y} - \boldsymbol{\mu} \boldsymbol{\nu}^T\|_F^2 + \left\| (\boldsymbol{\mu}^2 + \text{diag}(\mathbf{A})) (\boldsymbol{\nu}^2 + \text{diag}(\mathbf{B}))^T - \boldsymbol{\mu}^2 (\boldsymbol{\nu}^2)^T \right\|_{1,1} \right) \\ &\quad - \frac{N}{2} \log(2\pi) + \frac{N}{2} \log \beta - \frac{\beta}{2} (\|\boldsymbol{\mu} - F(\mathbf{X})\|_2^2 + \text{tr}(\mathbf{A})) \\ &\quad - \frac{M}{2} \log(2\pi) - \frac{1}{2} \|\boldsymbol{\nu}\|_2^2 - \frac{1}{2} \text{tr}(\mathbf{B}) \\ &\quad + \frac{N}{2} \log(2\pi) + \frac{1}{2} \log \det(\mathbf{A}) + \frac{N}{2} \\ &\quad + \frac{M}{2} \log(2\pi) + \frac{1}{2} \log \det(\mathbf{B}) + \frac{M}{2} \\ &= \frac{NM}{2} \log \tau - \frac{\tau}{2} \left(\|\mathbf{Y} - \boldsymbol{\mu} \boldsymbol{\nu}^T\|_F^2 + \left\| (\boldsymbol{\mu}^2 + \text{diag}(\mathbf{A})) (\boldsymbol{\nu}^2 + \text{diag}(\mathbf{B}))^T - \boldsymbol{\mu}^2 (\boldsymbol{\nu}^2)^T \right\|_{1,1} \right) \\ &\quad + \frac{N}{2} \log \beta - \frac{\beta}{2} (\|\boldsymbol{\mu} - F(\mathbf{X})\|_2^2 + Na^2) + \text{const},\end{aligned}\tag{52}$$

where $\text{diag}(\cdot)$ denotes the vector containing all the entries on the main diagonal of a squared matrix and $\text{tr}(\cdot)$ denotes the trace. We consider the model parameters first and fix the current estimate for $F(\cdot)$. Setting the derivative of (52) with respect to τ and β be 0, we

can obtain the estimation of these two parameters

$$\begin{aligned}\tau &= \frac{NM}{\|\mathbf{Y} - \boldsymbol{\mu}\boldsymbol{\nu}^T\|_F^2 + \left\|(\boldsymbol{\mu}^2 + \text{diag}(\mathbf{A}))(\boldsymbol{\nu}^2 + \text{diag}(\mathbf{B}))^T - \boldsymbol{\mu}^2(\boldsymbol{\nu}^2)^T\right\|_{1,1}}, \\ \beta &= \frac{N}{\|\boldsymbol{\mu} - F(\mathbf{X})\|_2^2 + Na^2}.\end{aligned}\tag{53}$$

Then we fix $\boldsymbol{\theta}$, and the ELBO can be written as

$$\text{ELBO} = -\frac{\beta}{2} \|\boldsymbol{\mu} - F(\mathbf{X})\|_2^2 + \text{const}.\tag{54}$$

Maximizing (54) with respect to $F(\cdot)$ is equivalent to solving the following optimization problem

$$\min_{F(\cdot)} \mathcal{L}(\boldsymbol{\mu}, F(\cdot)),\tag{55}$$

where

$$\mathcal{L}(\boldsymbol{\mu}, F(\cdot)) = \frac{\beta}{2} \|\boldsymbol{\mu} - F(\mathbf{X})\|_2^2.\tag{56}$$

Here we adopt the idea of the gradient boosting machine in each iteration to construct $F(\cdot)$. Suppose in the $(t-1)$ -th step, the current estimate for $F(\cdot)$ is denoted as $F^{(t-1)}(\cdot)$. Specifically, boosting finds a minimizer of the loss function $\mathcal{L}(\boldsymbol{\mu}, F(\cdot))$ in a stage-wise manner by sequentially adding an update $f^{(t)}(\cdot)$ to $F^{(t-1)}(\cdot)$ in the t -th step

$$F^{(t)}(\cdot) = F^{(t-1)}(\cdot) + f^{(t)}(\cdot),\tag{57}$$

where T is the total number of trees, and

$$f^{(t)}(\cdot) = \arg \min_{f(\cdot)} \mathcal{L}(\boldsymbol{\mu}, F^{(t-1)}(\cdot) + f(\cdot)),\tag{58}$$

is a single regression tree. With the adoption of the Newton boosting (Sigrüst, 2021), it's clear that the optimal solution for $f^{(t)}(\cdot)$ is given by

$$f^{(t)}(\cdot) = \arg \min_{f(\cdot)} \|\boldsymbol{\mu} - F^{(t-1)}(\mathbf{X}) - f(\mathbf{X})\|_2^2.\tag{59}$$

Further, it has been empirically observed that higher prediction accuracy can be obtained by damping the update (Friedman, 2001)

$$F^{(t)}(\cdot) = F^{(t-1)}(\cdot) + s \cdot f^{(t)}(\cdot),\tag{60}$$

where $0 < s < 1$ is the so-called shrinkage parameter or learning rate.

A.2 Missing Data

To handle \mathbf{Y} with missing entries, we consider the following probabilistic model for the observed entries \mathbf{Y}^{obs}

$$\begin{aligned} \Pr(\mathbf{Y}^{\text{obs}} \mid \boldsymbol{\theta}, F(\cdot)) &= \Pr(\mathbf{Y}^{\text{obs}} \mid \mathbf{z}, \mathbf{w}; \tau) \Pr(\mathbf{z} \mid \beta, F(\cdot)) \Pr(\mathbf{w}) \\ &= \left(\prod_{(n,m) \in \Omega^{\text{obs}}} \Pr(\mathbf{Y}_{nm} \mid \mathbf{z}, \mathbf{w}; \tau) \right) \Pr(\mathbf{z} \mid \beta, F(\cdot)) \Pr(\mathbf{w}), \end{aligned} \quad (61)$$

where Ω^{obs} is the collection of the indices of the observed entries. Then the log-likelihood function can be written as

$$\begin{aligned} \log \Pr(\mathbf{Y}^{\text{obs}}, \mathbf{z}, \mathbf{w} \mid \tau, \beta; F(\cdot)) &= \log \Pr(\mathbf{Y}^{\text{obs}} \mid \mathbf{z}, \mathbf{w}; \tau) + \log \Pr(\mathbf{z} \mid \beta; F(\cdot)) + \log \Pr(\mathbf{w}) \\ &= -\frac{|\Omega^{\text{obs}}|}{2} \log(2\pi) + \frac{|\Omega^{\text{obs}}|}{2} \log \tau - \frac{\tau}{2} \|\mathcal{P}_{\Omega^{\text{obs}}}(\mathbf{Y} - \mathbf{z}\mathbf{w}^{\text{T}})\|_{\text{F}}^2 \\ &\quad - \frac{N}{2} \log(2\pi) + \frac{N}{2} \log \beta - \frac{\beta}{2} \|\mathbf{z} - F(\mathbf{X})\|_2^2 \\ &\quad - \frac{M}{2} \log(2\pi) - \frac{1}{2} \|\mathbf{w}\|_2^2, \end{aligned} \quad (62)$$

where \mathcal{P} is a projection operator and $\mathcal{P}_{\Omega}(\mathbf{Y})$ outputs a matrix with the same dimension as that of \mathbf{Y}

$$(\mathcal{P}_{\Omega}(\mathbf{Y}))_{nm} = \begin{cases} \mathbf{Y}_{nm}, & \text{if } (n, m) \in \Omega, \\ 0, & \text{otherwise.} \end{cases} \quad (63)$$

To simplify the derivation and exploit standard fast matrix multiplication routines, we introduce the data precision matrix $\boldsymbol{\tau} \in \mathbb{R}^{N \times M}$ as follows

$$\boldsymbol{\tau}_{nm} = \begin{cases} \tau, & \text{if } (n, m) \in \Omega^{\text{obs}}, \\ 0, & \text{otherwise.} \end{cases} \quad (64)$$

Then similar to Section A.1, the optimal solutions of the variational approximate posteriors in the E-step are given as

$$\begin{aligned}
& \log q(\mathbf{z}) \\
&= \mathbb{E}_{q(\mathbf{w})} [\log \Pr(\mathbf{Y}^{\text{obs}}, \mathbf{z}, \mathbf{w})] + \text{const} \\
&= \mathbb{E}_{q(\mathbf{w})} \left[-\frac{\tau}{2} \|\mathcal{P}_{\Omega^{\text{obs}}}(\mathbf{Y} - \mathbf{z}\mathbf{w}^{\text{T}})\|_{\text{F}}^2 \right] - \frac{\beta}{2} \|\mathbf{z} - F(\mathbf{X})\|_2^2 + \text{const} \\
&= -\frac{1}{2} \sum_{m=1}^M \mathbb{E}_{q(\mathbf{w})} \left[(\mathbf{Y}_{\cdot m} - \mathbf{w}_m \mathbf{z})^{\text{T}} (\boldsymbol{\tau}_{\cdot m} \circ (\mathbf{Y}_{\cdot m} - \mathbf{w}_m \mathbf{z})) \right] - \frac{\beta}{2} (\mathbf{z} - F(\mathbf{X}))^{\text{T}} (\mathbf{z} - F(\mathbf{X})) + \text{const} \\
&= -\frac{1}{2} \mathbf{z}^{\text{T}} \left(\sum_{m=1}^M \mathbb{E}_{q(\mathbf{w})} [\mathbf{w}_m^2] \text{diag}(\boldsymbol{\tau}_{\cdot m}) \right) \mathbf{z} + \mathbf{z}^{\text{T}} \left(\sum_{m=1}^M \mathbb{E}_{q(\mathbf{w})} [\mathbf{w}_m] (\boldsymbol{\tau}_{\cdot m} \circ \mathbf{Y}_{\cdot m}) \right) \\
&\quad - \frac{\beta}{2} \mathbf{z}^{\text{T}} \mathbf{z} + \mathbf{z}^{\text{T}} (\beta F(\mathbf{X})) + \text{const} \\
&= -\frac{1}{2} \mathbf{z}^{\text{T}} \text{diag}(\beta + \boldsymbol{\tau} \mathbb{E}_{q(\mathbf{w})} [\mathbf{w}^2]) \mathbf{z} + \mathbf{z}^{\text{T}} (\beta F(\mathbf{X}) + (\boldsymbol{\tau} \circ \mathbf{Y}) \mathbb{E}_{q(\mathbf{w})} [\mathbf{w}]) + \text{const}, \\
& \log q(\mathbf{w}) \\
&= \mathbb{E}_{q(\mathbf{z})} [\log \Pr(\mathbf{Y}^{\text{obs}}, \mathbf{z}, \mathbf{w})] + \text{const} \\
&= \mathbb{E}_{q(\mathbf{z})} \left[-\frac{\tau}{2} \|\mathcal{P}_{\Omega^{\text{obs}}}(\mathbf{Y} - \mathbf{z}\mathbf{w}^{\text{T}})\|_{\text{F}}^2 \right] - \frac{1}{2} \|\mathbf{w}\|_2^2 + \text{const} \\
&= -\frac{1}{2} \sum_{n=1}^N \mathbb{E}_{q(\mathbf{z})} \left[(\mathbf{Y}_{n\cdot} - \mathbf{z}_n \mathbf{w})^{\text{T}} (\boldsymbol{\tau}_{n\cdot} \circ (\mathbf{Y}_{n\cdot} - \mathbf{z}_n \mathbf{w})) \right] - \frac{1}{2} \mathbf{w}^{\text{T}} \mathbf{w} + \text{const} \\
&= -\frac{1}{2} \mathbf{w}^{\text{T}} \left(\sum_{n=1}^N \mathbb{E}_{q(\mathbf{z})} [\mathbf{z}_n^2] \text{diag}(\boldsymbol{\tau}_{n\cdot}) \right) \mathbf{w} + \mathbf{w}^{\text{T}} \left(\sum_{n=1}^N \mathbb{E}_{q(\mathbf{z})} [\mathbf{z}_n] (\boldsymbol{\tau}_{n\cdot} \circ \mathbf{Y}_{n\cdot}) \right) - \frac{1}{2} \mathbf{w}^{\text{T}} \mathbf{w} + \text{const} \\
&= -\frac{1}{2} \mathbf{w}^{\text{T}} \text{diag}(1 + \boldsymbol{\tau}^{\text{T}} \mathbb{E}_{q(\mathbf{z})} [\mathbf{z}^2]) \mathbf{w} + \mathbf{w}^{\text{T}} \left((\boldsymbol{\tau} \circ \mathbf{Y})^{\text{T}} \mathbb{E}_{q(\mathbf{z})} [\mathbf{z}] \right) + \text{const}, \tag{65}
\end{aligned}$$

where \circ denotes the Hadamard product (i.e., element-wise product), $\mathbf{z}^2 = \mathbf{z} \circ \mathbf{z} \in \mathbb{R}^{N \times 1}$ and $\mathbf{w}^2 = \mathbf{w} \circ \mathbf{w} \in \mathbb{R}^{M \times 1}$, and $\text{diag}(\beta + \boldsymbol{\tau} \mathbb{E}_{q(\mathbf{w})} [\mathbf{w}^2]) \in \mathbb{R}^{M \times M}$ and $\text{diag}(1 + \boldsymbol{\tau}^{\text{T}} \mathbb{E}_{q(\mathbf{z})} [\mathbf{z}^2]) \in \mathbb{R}^{M \times M}$ are two diagonal matrices in which the main diagonal entries are equal to $\beta +$

$\boldsymbol{\tau} \mathbb{E}_{q(\mathbf{w})} [\mathbf{w}^2]$ and $1 + \boldsymbol{\tau}^T \mathbb{E}_{q(\mathbf{z})} [\mathbf{z}^2]$ respectively

$$\begin{aligned}
\text{diag}(\beta + \boldsymbol{\tau} \mathbb{E}_{q(\mathbf{w})} [\mathbf{w}^2]) &= \begin{bmatrix} \beta + \boldsymbol{\tau}_1^T \mathbb{E}_{q(\mathbf{w})} [\mathbf{w}^2] & & \\ & \ddots & \\ & & \beta + \boldsymbol{\tau}_N^T \mathbb{E}_{q(\mathbf{w})} [\mathbf{w}^2] \end{bmatrix} \\
&= \begin{bmatrix} \beta + \sum_{m=1}^M \boldsymbol{\tau}_{1m} \mathbb{E}_{q(\mathbf{w})} [\mathbf{w}_m^2] & & \\ & \ddots & \\ & & \beta + \sum_{m=1}^M \boldsymbol{\tau}_{Nm} \mathbb{E}_{q(\mathbf{w})} [\mathbf{w}_m^2] \end{bmatrix}, \\
\text{diag}(1 + \boldsymbol{\tau}^T \mathbb{E}_{q(\mathbf{z})} [\mathbf{z}^2]) &= \begin{bmatrix} 1 + \boldsymbol{\tau}_1^T \mathbb{E}_{q(\mathbf{z})} [\mathbf{z}^2] & & \\ & \ddots & \\ & & 1 + \boldsymbol{\tau}_M^T \mathbb{E}_{q(\mathbf{z})} [\mathbf{z}^2] \end{bmatrix} \\
&= \begin{bmatrix} 1 + \sum_{n=1}^N \boldsymbol{\tau}_{n1} \mathbb{E}_{q(\mathbf{z})} [\mathbf{z}_n^2] & & \\ & \ddots & \\ & & 1 + \sum_{n=1}^N \boldsymbol{\tau}_{nM} \mathbb{E}_{q(\mathbf{z})} [\mathbf{z}_n^2] \end{bmatrix}.
\end{aligned} \tag{66}$$

The quadratic forms (65) indicate that both \mathbf{z} and \mathbf{w} follow Gaussian distribution

$$q(\mathbf{z}) = \mathcal{N}_N(\mathbf{z} \mid \boldsymbol{\mu}, \mathbf{A}), \quad q(\mathbf{w}) = \mathcal{N}_M(\mathbf{w} \mid \boldsymbol{\nu}, \mathbf{B}), \tag{67}$$

where $\boldsymbol{\mu} \in \mathbb{R}^{N \times 1}$ and $\boldsymbol{\nu} \in \mathbb{R}^{M \times 1}$ are posterior mean vectors and $\mathbf{A} \in \mathbb{R}^{N \times N}$ and $\mathbf{B} \in \mathbb{R}^{M \times M}$ are covariance matrices

$$\begin{aligned}
\mathbf{A} &= \text{diag}(\mathbf{a}^2), \quad \boldsymbol{\mu} = \mathbf{A}(\beta F(\mathbf{X}) + (\boldsymbol{\tau} \circ \mathbf{Y}) \boldsymbol{\nu}), \\
\mathbf{B} &= \text{diag}(\mathbf{b}^2), \quad \boldsymbol{\nu} = \mathbf{B}(\boldsymbol{\tau} \circ \mathbf{Y})^T \boldsymbol{\mu},
\end{aligned} \tag{68}$$

where $\mathbf{a}^2 \in \mathbb{R}^{N \times 1}$ and $\mathbf{b}^2 \in \mathbb{R}^{M \times 1}$ are two vectors

$$\begin{aligned}
\mathbf{a}_n^2 &= \frac{1}{\beta + \boldsymbol{\tau}_n^T (\boldsymbol{\nu}^2 + \mathbf{b}^2)}, \quad \boldsymbol{\mu}_n = \mathbf{a}_n^2 \left(\beta F(\mathbf{X}_{n\cdot}) + (\boldsymbol{\tau}_{n\cdot} \circ \mathbf{Y}_{n\cdot})^T \boldsymbol{\nu} \right), \quad n = 1, \dots, N \\
\mathbf{b}_m^2 &= \frac{1}{1 + \boldsymbol{\tau}_{\cdot m}^T (\boldsymbol{\mu}^2 + \mathbf{a}^2)}, \quad \boldsymbol{\nu}_m = \mathbf{b}_m^2 (\boldsymbol{\tau}_{\cdot m} \circ \mathbf{Y}_{\cdot m})^T \boldsymbol{\mu}, \quad m = 1, \dots, M.
\end{aligned} \tag{69}$$

In the M-step, we turn to fix the variational approximate posterior $q(\mathbf{z}, \mathbf{w})$ and maximize the ELBO with respect to $\boldsymbol{\theta}$ and $F(\cdot)$. With (67), the ELBO is given by

$$\begin{aligned}
& \text{ELBO}(q; \tau, \beta; F(\cdot)) \\
&= \mathbb{E}_q [\log \Pr(\mathbf{Y}^{\text{obs}}, \mathbf{z}, \mathbf{w})] - \mathbb{E}_q [\log q(\mathbf{z}, \mathbf{w})] \\
&= -\frac{|\Omega^{\text{obs}}|}{2} \log(2\pi) + \frac{|\Omega^{\text{obs}}|}{2} \log \tau \\
&\quad - \frac{\tau}{2} \left(\|\mathcal{P}_{\Omega^{\text{obs}}}(\mathbf{Y} - \boldsymbol{\mu}\boldsymbol{\nu}^{\text{T}})\|_{\text{F}}^2 + \left\| \mathcal{P}_{\Omega^{\text{obs}}} \left((\boldsymbol{\mu}^2 + \text{diag}(\mathbf{A})) (\boldsymbol{\nu}^2 + \text{diag}(\mathbf{B}))^{\text{T}} - \boldsymbol{\mu}^2 (\boldsymbol{\nu}^2)^{\text{T}} \right) \right\|_{1,1} \right) \\
&\quad - \frac{N}{2} \log(2\pi) + \frac{N}{2} \log \beta - \frac{\beta}{2} (\|\boldsymbol{\mu} - F(\mathbf{X})\|_2^2 + \text{tr}(\mathbf{A})) \\
&\quad - \frac{M}{2} \log(2\pi) - \frac{1}{2} \|\boldsymbol{\nu}\|_2^2 - \frac{1}{2} \text{tr}(\mathbf{B}) \\
&\quad + \frac{N}{2} \log(2\pi) + \frac{1}{2} \log \det(\mathbf{A}) + \frac{N}{2} \\
&\quad + \frac{M}{2} \log(2\pi) + \frac{1}{2} \log \det(\mathbf{B}) + \frac{M}{2} \\
&= \frac{|\Omega^{\text{obs}}|}{2} \log \tau - \frac{\tau}{2} \left(\|\mathcal{P}_{\Omega^{\text{obs}}}(\mathbf{Y} - \boldsymbol{\mu}\boldsymbol{\nu}^{\text{T}})\|_{\text{F}}^2 + \left\| \mathcal{P}_{\Omega^{\text{obs}}} \left((\boldsymbol{\mu}^2 + \mathbf{a}^2) (\boldsymbol{\nu}^2 + \mathbf{b}^2)^{\text{T}} - \boldsymbol{\mu}^2 (\boldsymbol{\nu}^2)^{\text{T}} \right) \right\|_{1,1} \right) \\
&\quad + \frac{N}{2} \log \beta - \frac{\beta}{2} (\|\boldsymbol{\mu} - F(\mathbf{X})\|_2^2 + \|\mathbf{a}^2\|_1) + \text{const}, \tag{70}
\end{aligned}$$

where $\text{diag}(\cdot)$ denotes the vector containing all the entries on the main diagonal of a squared matrix and $\text{tr}(\cdot)$ denotes the trace. We consider the model parameters first and fix the current estimate for $F(\cdot)$. Setting the derivative of (70) with respect to τ and β be 0, we can obtain the estimation of these two parameters

$$\begin{aligned}
\tau &= \frac{|\Omega^{\text{obs}}|}{\|\mathcal{P}_{\Omega^{\text{obs}}}(\mathbf{Y} - \boldsymbol{\mu}\boldsymbol{\nu}^{\text{T}})\|_{\text{F}}^2 + \left\| \mathcal{P}_{\Omega^{\text{obs}}} \left((\boldsymbol{\mu}^2 + \mathbf{a}^2) (\boldsymbol{\nu}^2 + \mathbf{b}^2)^{\text{T}} - \boldsymbol{\mu}^2 (\boldsymbol{\nu}^2)^{\text{T}} \right) \right\|_{1,1}}, \\
\beta &= \frac{N}{\|\boldsymbol{\mu} - F(\mathbf{X})\|_2^2 + \|\mathbf{a}^2\|_1}. \tag{71}
\end{aligned}$$

The remaining part is the same as in Section A.1.

B Human Brain Gene Expression Data

The human brain gene expression dataset was generated from 1,340 tissue samples collected from 57 developing and adult post-mortem brains of clinically unremarkable donors

representing males and females of multiple ethnicities (Johnson et al., 2009; Kang et al., 2011).

B.1 Spatial and Temporal Information

A 15-period system spanning the periods from embryonic development to late adulthood was created to investigate the spatial-temporal dynamics of the human brain transcriptome (Table 3). The transient prenatal structures and immature and mature forms of 16 brain

Period	Description	Age
1	Embryonic	4 PCW \leq Age $<$ 8 PCW
2	Early fetal	8 PCW \leq Age $<$ 10 PCW
3	Early fetal	10 PCW \leq Age $<$ 13 PCW
4	Early mid-fetal	13 PCW \leq Age $<$ 16 PCW
5	Early mid-fetal	16 PCW \leq Age $<$ 19 PCW
6	Late mid-fetal	19 PCW \leq Age $<$ 24 PCW
7	Late fetal	24 PCW \leq Age $<$ 38 PCW
8	Neonatal and early infancy	0 M (birth) \leq Age $<$ 6 M
9	Late infancy	6M \leq Age $<$ 12 M
10	Early childhood	1 Y \leq Age $<$ 6 Y
11	Middle and late childhood	6 Y \leq Age $<$ 12 Y
12	Adolescence	12 Y \leq Age $<$ 20 Y
13	Young adulthood	20 Y \leq Age $<$ 40 Y
14	Middle adulthood	40 Y \leq Age $<$ 60 Y
15	Late adulthood	60 Y \leq Age

M, postnatal months; PCW, post-conceptual weeks; Y, postnatal years.

Table 3: Periods of human development and adulthood as defined in Johnson et al. (2009); Kang et al. (2011).

regions, including 11 neocortex areas, were sampled from multiple specimens per period (Table 4). It's obvious that periods 1 and 2 correspond to embryonic and early fetal devel-

Periods 1 and 2	Periods 3-15
FC, frontal cerebral wall	OFC, orbital prefrontal cortex DFC, dorsolateral prefrontal cortex VFC, ventrolateral prefrontal cortex MFC, medial prefrontal cortex M1C, primary motor (M1) cortex
PC, parietal cerebral wall	S1C, primary somatosensory (S1) cortex IPC, posterior inferior parietal cortex
TC, temporal cerebral wall	A1C, primary auditory (A1) cortex STC, superior temporal cortex ITC, inferior temporal cortex
OC, occipital cerebral wall	V1C, primary visual (V1) cortex
HIP, hippocampal anlage	HIP, hippocampus
—	AMY, amygdala
VF, ventral forebrain	STR, striatum
MGE, medial ganglionic eminence	
LGE, lateral ganglionic eminence	
CGE, caudal ganglionic eminence	
DIE, diencephalon	MD, mediodorsal nucleus of the thalamus
DTH, dorsal thalamus	—
URL, upper (rostral) rhombic lip	CBC, cerebellar cortex

Table 4: Ontology and nomenclature of analyzed brain regions and neocortex areas in [Johnson et al. \(2009\)](#); [Kang et al. \(2011\)](#).

opment when most of the 16 brain regions sampled in future periods have not differentiated (i.e., most of the 16 brain regions are missing data in periods 1 and 2). Therefore, data in periods 1 and 2 are excluded from our analysis. In this article, we focus on analyzing the neocortex areas, including the orbital prefrontal cortex (OFC), dorsolateral prefrontal cortex (DFC), ventrolateral prefrontal cortex (VFC), medial prefrontal cortex (MFC), pri-

mary motor cortex (M1C), primary somatosensory cortex (S1C), posterior inferior parietal cortex (IPC), primary auditory cortex (A1C), posterior superior temporal cortex (STC), inferior temporal cortex (ITC), and primary visual cortex (V1C).

B.2 Differential Stability

Differential stability (DS) is defined as the tendency for a gene to exhibit reproducible differential expression relationships across brain structures (Shaw et al., 2011). DS can be measured by a variety of different means, such as the average Kendall-Tau correlation, average Spearman correlation, and average Euclidean difference (see Hawrylycz et al. (2015) Supplementary Analysis for comparable metrics). Here we use the average Pearson correlation as an example. Suppose the whole brain gene expression dataset contains B individual brains and we need to calculate the average Pearson correlation over $B(B - 1)/2$ pairs of B brains to measure DS between brains. We can represent the previous gene expression data matrix to a tensor $\mathbf{X} \in \mathbb{R}^{B \times S \times G}$, where B denotes the individual brains, S denotes the anatomic structures (refer to the neocortex areas in our analysis), and G denotes the genes as in the main text. For each gene g expressed in a pair of brains (indexed by i and j) $\mathbf{X}_{i,g}$ and $\mathbf{X}_{j,g}$ with common anatomic structures S , we computed the Pearson correlation $\rho_S(\mathbf{X}_{i,g}, \mathbf{X}_{j,g})$. Then the DS of gene g is defined as the average ρ_S over $B(B - 1)/2$ pairs of brains. In summary, DS is a correlation-based metric that can be applied to assess the reproducibility of gene expression patterns across various structures in various individual brains and help reveal mesoscale genetic organization. Recent studies have shown that the genes with the highest DS are highly biologically relevant, with enrichment for brain-related annotations, disease associations, drug targets, and literature citations.

References

Agarwal, D. and B.-C. Chen (2009). Regression-based latent factor models. In *Proceedings of the 15th ACM SIGKDD International Conference on Knowledge Discovery and Data Mining*, pp. 19–28.

- Babacan, S. D., M. Luessi, R. Molina, and A. K. Katsaggelos (2012). Sparse bayesian methods for low-rank matrix estimation. *IEEE Transactions on Signal Processing* 60(8), 3964–3977.
- Bell, R. M. and Y. Koren (2007). Lessons from the netflix prize challenge. *ACM SIGKDD Explorations Newsletter* 9(2), 75–79.
- Belousov, A. B. and J. D. Fontes (2013). Neuronal gap junctions: making and breaking connections during development and injury. *Trends in Neurosciences* 36(4), 227–236.
- Bishop, C. M. (2006). *Pattern recognition and machine learning*. Springer.
- Blei, D. M., A. Kucukelbir, and J. D. McAuliffe (2017). Variational inference: A review for statisticians. *Journal of the American Statistical Association* 112(518), 859–877.
- Breiman, L. (1998). Arcing classifier (with discussion and a rejoinder by the author). *The Annals of Statistics* 26(3), 801–849.
- Breiman, L. and J. H. Friedman (1985). Estimating optimal transformations for multiple regression and correlation. *Journal of the American Statistical Association* 80(391), 580–598.
- Breiman, L., J. H. Friedman, R. A. Olshen, and C. J. Stone (1984). *Classification and Regression Trees*.
- Bühlmann, P. and T. Hothorn (2007). Boosting algorithms: Regularization, prediction and model fitting. *Statistical Science* 22(4), 477–505.
- Cai, J.-F., E. J. Candès, and Z. Shen (2010). A singular value thresholding algorithm for matrix completion. *SIAM Journal on Optimization* 20(4), 1956–1982.
- Candès, E. J. and B. Recht (2009). Exact matrix completion via convex optimization. *Foundations of Computational Mathematics* 9(6), 717–772.
- Candès, E. J. and T. Tao (2010). The power of convex relaxation: Near-optimal matrix completion. *IEEE Transactions on Information Theory* 56(5), 2053–2080.

- Cortes, D. (2018). Cold-start recommendations in collective matrix factorization. *arXiv preprint arXiv:1809.00366*.
- de Lores Arnaiz, G. R. and M. G. L. Ordieres (2014). Brain na^+ , k^+ -atpase activity in aging and disease. *International Journal of Biomedical Science* 10(2), 85.
- Elith, J., J. R. Leathwick, and T. Hastie (2008). A working guide to boosted regression trees. *Journal of Animal Ecology* 77(4), 802–813.
- Fithian, W. and R. Mazumder (2018). Flexible low-rank statistical modeling with missing data and side information. *Statistical Science* 33(2), 238–260.
- Freund, Y., R. E. Schapire, et al. (1996). Experiments with a new boosting algorithm. In *Proceedings of the Thirteenth International Conference on International Conference on Machine Learning*, San Francisco, CA, USA, pp. 148–156. Morgan Kaufmann Publishers Inc.
- Friedman, J., T. Hastie, and R. Tibshirani (2000). Additive logistic regression: a statistical view of boosting (with discussion and a rejoinder by the authors). *The Annals of Statistics* 28(2), 337–407.
- Friedman, J. H. (2001). Greedy function approximation: A gradient boosting machine. *The Annals of Statistics* 29(5), 1189–1232.
- Grinsztajn, L., E. Oyallon, and G. Varoquaux (2022). Why do tree-based models still outperform deep learning on typical tabular data? In *Thirty-sixth Conference on Neural Information Processing Systems Datasets and Benchmarks Track*.
- Harper, F. M. and J. A. Konstan (2015). The movielens datasets: History and context. *ACM Transactions on Interactive Intelligent Systems* 5(4), 1–19.
- Hastie, T., R. Mazumder, J. D. Lee, and R. Zadeh (2015). Matrix completion and low-rank svd via fast alternating least squares. *Journal of Machine Learning Research* 16(104), 3367–3402.

- Hawrylycz, M., J. A. Miller, V. Menon, D. Feng, T. Dolbeare, A. L. Guillozet-Bongaarts, A. G. Jegga, B. J. Aronow, C.-K. Lee, A. Bernard, M. F. Glasser, D. L. Dierker, J. Menche, A. Szafer, F. Collman, P. Grange, K. A. Berman, S. Mihalas, Z. Yao, L. Stewart, A.-L. Barabási, J. Schulkin, J. Phillips, L. Ng, C. Dang, D. R. Haynor, A. Jones, D. C. Van Essen, C. Koch, and E. Lein (2015). Canonical genetic signatures of the adult human brain. *Nature Neuroscience* 18(12), 1832–1844.
- Hubbard, C. and C. Hegde (2017). Parallel computing heuristics for low-rank matrix completion. In *2017 IEEE Global Conference on Signal and Information Processing (GlobalSIP)*, pp. 764–768. IEEE.
- Jain, P., P. Netrapalli, and S. Sanghavi (2013). Low-rank matrix completion using alternating minimization. In *Proceedings of the Forty-Fifth Annual ACM Symposium on Theory of Computing*, pp. 665–674.
- Johnson, M. B., Y. I. Kawasawa, C. E. Mason, Ž. Krsnik, G. Coppola, D. Bogdanović, D. H. Geschwind, S. M. Mane, M. W. State, and N. Šestan (2009). Functional and evolutionary insights into human brain development through global transcriptome analysis. *Neuron* 62(4), 494–509.
- Kang, H. J., Y. I. Kawasawa, F. Cheng, Y. Zhu, X. Xu, M. Li, A. M. M. Sousa, M. Pletikos, K. A. Meyer, G. Sedmak, T. Guennel, Y. Shin, M. B. Johnson, Ž. Krsnik, S. Mayer, S. Fertuzinhos, S. Umlauf, S. N. Lisgo, A. Vortmeyer, D. R. Weinberger, S. Mane, T. M. Hyde, A. Huttner, M. Reimers, J. E. Kleinman, and N. Šestan (2011). Spatio-temporal transcriptome of the human brain. *Nature* 478(7370), 483–489.
- Kinjo, É. R., R. M. Arida, D. M. de Oliveira, and M. J. da Silva Fernandes (2007). The na^+/k^+ atpase activity is increased in the hippocampus after multiple status epilepticus induced by pilocarpine in developing rats. *Brain Research* 1138, 203–207.
- Koren, Y., R. Bell, and C. Volinsky (2009). Matrix factorization techniques for recommender systems. *Computer* 42(8), 30–37.

- Lin, Z., S. J. Sanders, M. Li, N. Sestan, M. W. State, and H. Zhao (2015). A markov random field-based approach to characterizing human brain development using spatial–temporal transcriptome data. *The Annals of Applied Statistics* 9(1), 429–451.
- Lin, Z., T. Wang, C. Yang, and H. Zhao (2017). On joint estimation of gaussian graphical models for spatial and temporal data. *Biometrics* 73(3), 769–779.
- Lin, Z., C. Yang, Y. Zhu, J. Duchi, Y. Fu, Y. Wang, B. Jiang, M. Zamanighomi, X. Xu, M. Li, et al. (2016). Simultaneous dimension reduction and adjustment for confounding variation. *Proceedings of the National Academy of Sciences* 113(51), 14662–14667.
- Liu, T., M. Yuan, and H. Zhao (2022). Characterizing spatiotemporal transcriptome of the human brain via low-rank tensor decomposition. *Statistics in Biosciences* 14(3), 485–513.
- López-Otín, C., M. A. Blasco, L. Partridge, M. Serrano, and G. Kroemer (2013). The hallmarks of aging. *Cell* 153(6), 1194–1217.
- Luebke, J., Y.-M. Chang, T. Moore, and D. Rosene (2004). Normal aging results in decreased synaptic excitation and increased synaptic inhibition of layer 2/3 pyramidal cells in the monkey prefrontal cortex. *Neuroscience* 125(1), 277–288.
- Luebke, J. I. and D. L. Rosene (2003). Aging alters dendritic morphology, input resistance, and inhibitory signaling in dentate granule cells of the rhesus monkey. *Journal of Comparative Neurology* 460(4), 573–584.
- Mason, L., J. Baxter, P. Bartlett, and M. Frean (1999). Boosting algorithms as gradient descent. In *Proceedings of the 12th International Conference on Neural Information Processing Systems*, pp. 512–518.
- Mazumder, R., T. Hastie, and R. Tibshirani (2010). Spectral regularization algorithms for learning large incomplete matrices. *Journal of Machine Learning Research* 11(80), 2287–2322.

- Montoro, R. J. and R. Yuste (2004). Gap junctions in developing neocortex: a review. *Brain Research Reviews* 47(1-3), 216–226.
- Neal, R. M. (1993). *Probabilistic inference using Markov chain Monte Carlo methods*. Department of Computer Science, University of Toronto, Toronto, ON, Canada.
- Park, S., Y.-D. Kim, and S. Choi (2013). Hierarchical bayesian matrix factorization with side information. In *Proceedings of the Twenty-Third International Joint Conference on Artificial Intelligence*, pp. 1593–1599.
- Porteous, I., A. Asuncion, and M. Welling (2010). Bayesian matrix factorization with side information and dirichlet process mixtures. In *Proceedings of the Twenty-Fourth AAAI Conference on Artificial Intelligence*, Volume 24, pp. 563–568.
- Rasmussen, R., J. O’Donnell, F. Ding, and M. Nedergaard (2020). Interstitial ions: A key regulator of state-dependent neural activity? *Progress in Neurobiology* 193, 101802.
- Rennie, J. D. and N. Srebro (2005). Fast maximum margin matrix factorization for collaborative prediction. In *Proceedings of the 22nd International Conference on Machine Learning*, pp. 713–719.
- Salakhutdinov, R. and A. Mnih (2007). Probabilistic matrix factorization. In *Proceedings of the 20th International Conference on Neural Information Processing Systems*, pp. 1257–1264.
- Salakhutdinov, R. and A. Mnih (2008). Bayesian probabilistic matrix factorization using markov chain monte carlo. In *Proceedings of the 25th International Conference on Machine Learning*, pp. 880–887.
- Shang, L. and X. Zhou (2022). Spatially aware dimension reduction for spatial transcriptomics. *Nature Communications* 13(1), 7203.
- Shaw, G. T., E. S. Shih, C.-H. Chen, and M.-J. Hwang (2011). Preservation of ranking order in the expression of human housekeeping genes. *PLoS ONE* 6(12), e29314.

- Sigrist, F. (2021). Gradient and newton boosting for classification and regression. *Expert Systems With Applications* 167, 114080.
- Sigrist, F. (2022a). Gaussian process boosting. *Journal of Machine Learning Research* 23(232), 1–46.
- Sigrist, F. (2022b). Latent gaussian model boosting. *IEEE Transactions on Pattern Analysis and Machine Intelligence* 45(2), 1894–1905.
- Singh, A. P. and G. J. Gordon (2008). Relational learning via collective matrix factorization. In *Proceedings of the 14th ACM SIGKDD International Conference on Knowledge Discovery and Data Mining*, pp. 650–658.
- Srebro, N., J. D. Rennie, and T. S. Jaakkola (2004). Maximum-margin matrix factorization. In *Proceedings of the 17th International Conference on Neural Information Processing Systems*, pp. 1329–1336.
- Sutor, B. and T. Hagerty (2005). Involvement of gap junctions in the development of the neocortex. *Biochimica et Biophysica Acta (BBA)-Biomembranes* 1719(1-2), 59–68.
- Takács, G., I. Pilászy, B. Németh, and D. Tikk (2009). Scalable collaborative filtering approaches for large recommender systems. *Journal of Machine Learning Research* 10(22), 623–656.
- Therneau, T. and B. Atkinson (2022a). *rpart: Recursive Partitioning and Regression Trees*. R package version 4.1.19.
- Therneau, T. M. and E. J. Atkinson (2022b). An introduction to recursive partitioning using the rpart routines. Technical report, Mayo Foundation.
- Velten, B., J. M. Braunger, R. Argelaguet, D. Arnol, J. Wirbel, D. Bredikhin, G. Zeller, and O. Stegle (2022). Identifying temporal and spatial patterns of variation from multimodal data using mefisto. *Nature Methods* 19(2), 179–186.
- Wang, W. and M. Stephens (2021). Empirical bayes matrix factorization. *Journal of Machine Learning Research* 22(120), 1–40.

- Wen, Z., W. Yin, and Y. Zhang (2012). Solving a low-rank factorization model for matrix completion by a nonlinear successive over-relaxation algorithm. *Mathematical Programming Computation* 4(4), 333–361.
- Xu, M., R. Jin, and Z.-H. Zhou (2013). Speedup matrix completion with side information: application to multi-label learning. In *Proceedings of the 26th International Conference on Neural Information Processing Systems*, pp. 2301–2309.
- Yang, C., L. Wang, S. Zhang, and H. Zhao (2013). Accounting for non-genetic factors by low-rank representation and sparse regression for eqtl mapping. *Bioinformatics* 29(8), 1026–1034.
- Zakeri, P., J. Simm, A. Arany, S. ElShal, and Y. Moreau (2018). Gene prioritization using bayesian matrix factorization with genomic and phenotypic side information. *Bioinformatics* 34(13), i447–i456.
- Zhou, X., C. Yang, and W. Yu (2012). Moving object detection by detecting contiguous outliers in the low-rank representation. *IEEE Transactions on Pattern Analysis and Machine Intelligence* 35(3), 597–610.
- Zhou, X., C. Yang, H. Zhao, and W. Yu (2014). Low-rank modeling and its applications in image analysis. *ACM Computing Surveys* 47(2), 1–33.
- Zilber, P. and B. Nadler (2022). Inductive matrix completion: No bad local minima and a fast algorithm. In *Proceedings of the 39th International Conference on Machine Learning*, Volume 162, pp. 27671–27692. PMLR.